Multidimensional Spectroscopy

International Edition: DOI: 10.1002/anie.201502974
German Edition: DOI: 10.1002/ange.201502974

Multidimensional Electronic Spectroscopy of Photochemical Reactions

*Patrick Nuernberger, Stefan Ruetzel, and Tobias Brixner**

Keywords:
femtosecond two-dimensional spectroscopy · merocyanines · molecular switches · photochemistry · time-resolved spectroscopy

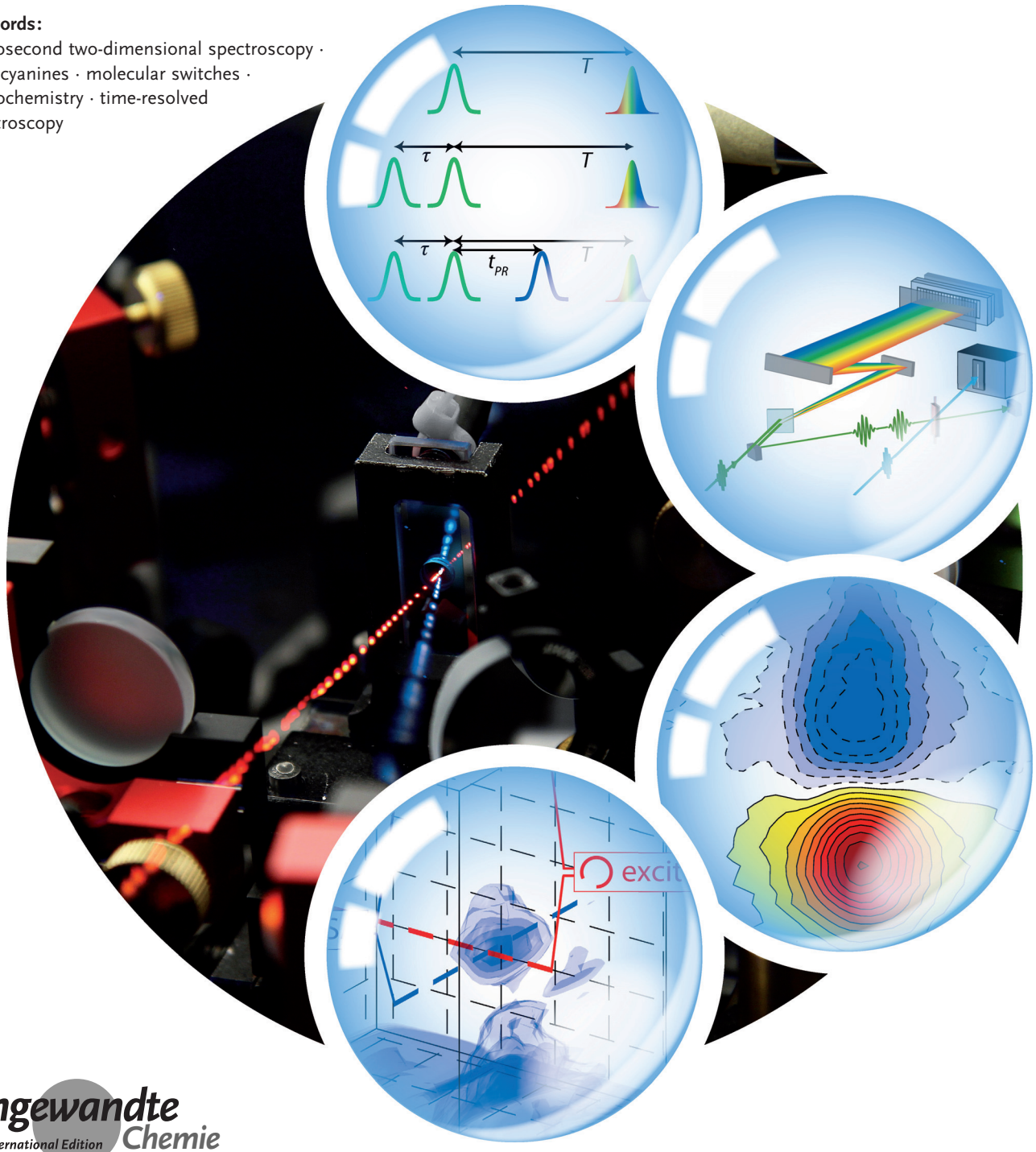

Coherent multidimensional electronic spectroscopy can be employed to unravel various channels in molecular chemical reactions. This approach is thus not limited to analysis of energy transfer or charge transfer (i.e. processes from photophysics), but can also be employed in situations where the investigated system undergoes permanent structural changes (i.e. in photochemistry). Photochemical model reactions are discussed by using the example of merocyanine/spiropyran-based molecular switches, which show a rich variety of reaction channels, in particular ring opening and ring closing, cis–trans isomerization, coherent vibrational wave-packet motion, radical ion formation, and population relaxation. Using pump-probe, pump-repump-probe, coherent two-dimensional and three-dimensional, triggered-exchange 2D, and quantum-control spectroscopy, we gain intuitive pictures on which product emerges from which reactant and which reactive molecular modes are associated.

From the Contents

1. Introduction

Spectroscopic approaches that map out a characteristic signal not only as a function of one external parameter but rather of several ones generally provide more insight into the underlying physics. As a main benefit, one can often separate contributions that would be overlapping in a one-dimensional measurement. The power of multidimensional techniques lies in the disclosure of a connection between an initially excited and a successively probed behavior. This can, for example, be achieved by a sequence of electromagnetic pulses that interact with the sample several times. By recording the system's response as a function of pulse delays and subsequent Fourier transformation, two frequency axes connected to the excitation and probing step are obtained. Such a coherent two-dimensional (2D) spectroscopy procedure has proven extremely versatile for a variety of processes and various spectral regimes of electromagnetic radiation. In nuclear magnetic resonance (NMR)[1–3] using radio waves, numerous implementations in two (or more) dimensions have been developed which facilitate the identification of spin–spin couplings of two nuclei, either through space or through chemical bonds, thus making microscopic structural information on the system accessible. The microwave implementations in electron paramagnetic resonance (EPR)[4,5] are extremely sensitive measures of coupling between electrons and reveal orientational details even in large biomolecular systems. As the most recent development, optical coherent 2D spectroscopy, described in a number of books[6–9] and review articles,[10–16] has been realized for vibrational (mid-infrared spectral region, see Refs. [8,9,15,17–26] and references therein) and electronic transitions (near-infrared to ultraviolet, see, for example, Refs. [27–46] and further references throughout this Review). This femtosecond technique and its variants open up unprecedented possibilities to study ultrafast processes in numerous systems, from small molecules to large protein complexes and from isolated atoms to bulk behavior in semiconductors.

Coherent 2D spectroscopy of electronic transitions is employed very successfully, in particular, for the study of natural and artificial light-harvesting systems. Starting with the first experiment on a multichromophore system,[33] there are now hundreds of publications in the field dealing with various aspects of electronic couplings and exciton dynamics. Many of these applications of electronic 2D spectroscopy have been reviewed recently.[10–15] These studies show impressively that photophysical dynamics can be resolved with unprecedented detail. Following complex excited-state dynamics, such as energy transfer, the system ultimately relaxes back to its initial ground state (Figure 1, left).

In contrast to these well-established applications of 2D spectroscopy to photophysical phenomena, we focus in the present Review on photochemistry (Figure 1, right). In this case, the geometric structure of the product is different from the reactant, such as in *cis–trans* isomerization or bond-

[*] Dr. S. Ruetzel, Prof. Dr. T. Brixner
Institut für Physikalische und Theoretische Chemie
Universität Würzburg
Am Hubland, 97074 Würzburg (Germany)
E-mail: brixner@phys-chemie.uni-wuerzburg.de
Prof. Dr. P. Nuernberger
Fakultät für Chemie und Biochemie
Ruhr-Universität Bochum
Universitätsstrasse 150, 44801 Bochum (Germany)

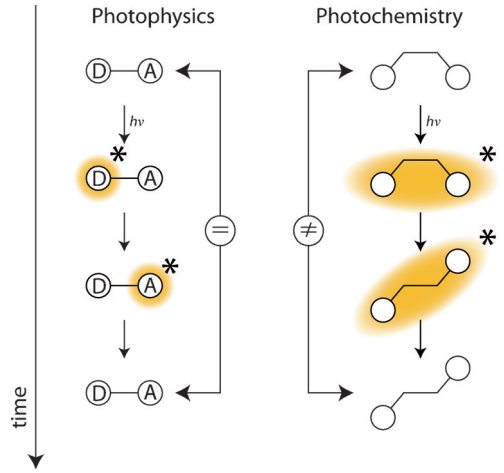

Figure 1. Abridged illustration of photophysical versus photochemical molecular processes. Photophysical phenomena (left) are characterized by purely physical changes occurring after irradiation with light, as exemplified here by energy transport from a donor (D) to an acceptor (A) subunit. Although the transiently formed photoexcited species may exhibit different spectral properties than the ground-state species, no permanent change remains after relaxation back to its original ground state. In contrast, the term photochemistry (right) is referred to here as a (light-induced) reaction in which a product species is formed in its thermodynamically stable electronic ground state, which possesses a molecular configuration different from that of the reactant.

breaking reactions. The question thus arises how this complicates the data analysis because the accessible electronic states at the beginning of the femtosecond pulse sequence are different from those at the end. We will show, nevertheless, that 2D spectroscopy and its variants provide powerful tools to analyze ultrafast photochemical reactions.

To illustrate the potential of 2D spectroscopy, we have chosen a merocyanine/spiropyran model system with rich photochemical behavior. As a molecular switch, the system can potentially undergo ring-closure and ring-opening reactions as well as *cis–trans* isomerization or ionization. We will apply a series of time-resolved spectroscopic techniques with increasing complexity, namely, more and more complex pulse sequences to access nonlinearities from first order over third to fifth and potentially even higher order. Since all the techniques will be tested on the same molecular system, a comprehensive picture emerges for which each technique provides further pieces of either confirmative or complementary information.

2. Pulse Sequences in Femtochemistry

In the field of ultrafast spectroscopy, a large variety of different experimental techniques have been developed to probe photochemical dynamics on femtosecond timescales.[6,47–49] In general, one femtosecond laser pulse triggers a reaction, and at least one second pulse is used to probe the ensuing dynamics. Possible signals are transient changes in absorption or fluorescence, ionization mass spectra, photoelectron distributions, or other observables as a function of time elapsed since the interaction with the initial laser pulse. In the following we will give a brief overview of pulse sequences employed in the field of femtochemistry (Figure 2) which rely on (changing) absorption signals and which are relevant for the studies described in this Review. We employ a density-matrix terminology to point out the differences, but analogous descriptions are possible using a wave-packet picture.

In steady-state absorption measurements (Figure 2a) a single interaction with the electrical field of the light allows for the detection of the linear absorption spectrum, thus probing the first-order electric susceptibility tensor $\chi^{(1)}$ without yielding any explicit temporal resolution, even if the employed light is pulsed.

In ultrafast spectroscopy, temporal resolution is achieved by employing several short laser pulses which interact with the sample, some of them even multiple times. Therefore, the investigated processes are nonlinear in nature, that is, more than one interaction with the light fields is required. The number of interactions determines the order of the susceptibility tensor giving rise to the observed signal, as illustrated in Figure 2.

For many years pump-probe techniques such as transient absorption (Figure 2b) have dominated the field. A femtosecond pump pulse excites the sample and a probe pulse, delayed by the pump-probe delay T, is used to monitor the photodynamics as a function of T. A third-order signal (i.e. in

Patrick Nuernberger studied physics at the University of Würzburg and the State University of New York at Stony Brook. From 2008 to 2010, he was a postdoctoral fellow at Ecole Polytechnique, France. He then started a junior research group at the Institute of Physical and Theoretical Chemistry at the University of Würzburg, for which he was awarded an Emmy-Noether grant by the DFG. He completed his habilitation in 2013, and since 2014 has been a professor of physical chemistry at the Ruhr-University Bochum. His research focuses on investigating femtosecond dynamics and photochemical reactions with advanced ultrafast spectroscopic methods and quantum control approaches.

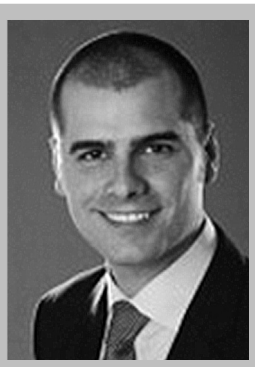

Stefan Ruetzel was born in 1983 and studied physics at the University of Würzburg. He joined the research group of Prof. Tobias Brixner and received his MSc in 2009. His graduate studies mainly focused on the investigation of ultrafast photochemical reactions with multidimensional electronic spectroscopy. He received his PhD with distinction in 2014 and is currently a postdoctoral researcher in the group of Tobias Brixner.

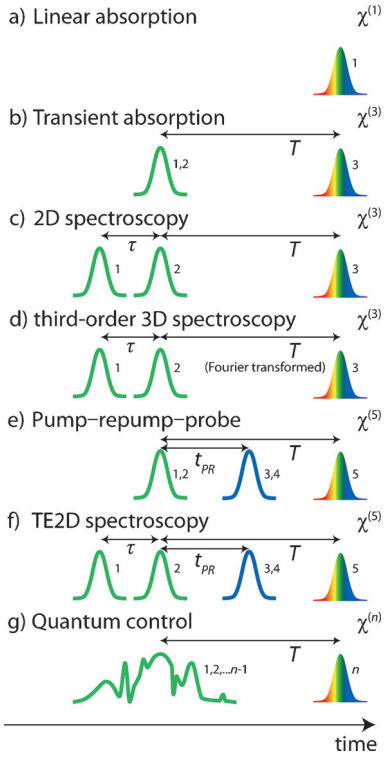

Figure 2. Femtosecond spectroscopy approaches, the associated pulse sequences, and the probed susceptibility tensor. The small numbers indicate the sequence of interactions of the light fields with the sample. a) No time resolution is achieved with linear absorption. b) Transient absorption, c) coherent 2D, and d) third-order 3D spectroscopy have in common that three field interactions occur, which is why these approaches are third-order techniques. e) An additional repump pulse is used in pump-repump-probe and f) triggered-exchange 2D spectroscopy and thus these techniques probe the fifth-order nonlinear susceptibility tensor. g) In quantum-control spectroscopy, a shaped femtosecond laser pulse is used and multiple field interactions (of undetermined order) may occur.

third order with respect to the laser field as analyzed within perturbation theory) is observed since the pump pulse interacts twice with the sample, thereby creating a population in the excited state followed by a single interaction with the probe. The quantity determined in these experiments is thus proportional to the third-order nonlinear susceptibility tensor $\chi^{(3)}$.

Coherent two-dimensional (2D) spectroscopy is often referred to as the optical analogue of two-dimensional nuclear magnetic resonance (2D NMR).[1–3] In the Fourier-transform approach to coherent optical 2D spectroscopy, three laser pulses interact with the sample (Figure 2c). Thus, the first pulse creates a coherence between the ground and the excited state while the interaction with a second pulse, delayed by the coherence time τ, converts the coherence into a ground- or excited-state population. There is also the possibility that a coherence is reached after two interactions, as in double-quantum coherence 2D spectroscopy.[50–54] Furthermore, coherent wave-packet motion can be induced as well, as will be important in 3D spectroscopy (see Section 8). The probe pulse provides the third interaction after the population time (also called waiting time) T, similar to the pump-probe delay in transient absorption. The nonlinear signal emerges as a function of a second coherence time t. Fourier transformation along both τ and t then leads to 2D spectra for each time parameter T. In most implementations, the first Fourier transformation along τ is performed numerically on the computer, while the second Fourier transformation along t is performed implicitly by detecting the signal with a spectrometer. Phase information is retrieved by coherent superposition with a known reference pulse (i.e. spectral interferometry). In this manner, a 2D spectrum is obtained which spreads the time-resolved data along two independent frequency axes. This allows for the detection of correlations and couplings between different spectral contributions.

Third-order three-dimensional (3D) spectroscopy (Figure 2d) is implemented with the same pulse sequence as coherent 2D spectroscopy.[55–61] By collecting a series of 2D spectra at variable population times and by taking the Fourier transform also along T, a third-order 3D spectrum is obtained. This 3D spectrum resolves the response of the system not only along the pump and probe frequency axis but also along a third frequency axis associated with oscillations that occur during the population time. Such oscillations may be caused, for example, by a double-quantum coherence or by coherent vibrational motion during or after a photoreaction. In recent years, the observation of long-living coherent oscillations in the photophysical 2D spectra of excitonically coupled systems (particularly in light-harvesting systems) has been under vivid debate in regard to the vibrational and/or electronic nature of these signatures.[36,41,61–80] Therefore, to facilitate the discussion of newly established methods, we chose a molecular model system without any excitonic couplings, where signal oscillations can be attributed to purely vibrational origins.

In pump-repump-probe spectroscopy (Figure 2e) the pump pulse creates an excited-state population which is either reexcited to even higher-lying states[81–85] or dumped to lower intermediate or product states,[86–91] an approach also known from quantum control.[92–94] Experimentally, the pump-probe scheme is expanded by a third laser pulse that is delayed by the pump-repump delay t_{PR} with respect to the pump, thus making this method a fifth-order technique. The probe pulse monitors absorption changes induced by either

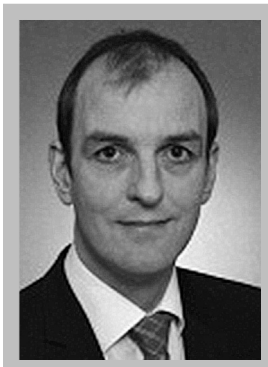

Tobias Brixner studied physics at the University of Würzburg and the University of New Mexico at Albuquerque. He received his PhD in the group of Prof. Gustav Gerber. During his postdoctoral stay in 2003/2004 with Prof. Graham R. Fleming (University of California at Berkeley), he developed coherent 2D spectroscopy for the visible regime and then returned to Würzburg to establish an Emmy-Noether Junior Group. Since 2007 he has held a Chair for Physical Chemistry at Würzburg. His current research interests include method development and applications in 2D spectroscopy, quantum control, and ultrafast nanooptics.

solely pump or repump pulses as well as those caused cooperatively by both of them. This latter signal is the desired one and can be isolated with pulse-chopping techniques.

Triggered-exchange 2D (TE2D) spectroscopy (Figure 2 f) is a combination of pump-repump-probe and 2D spectroscopy and is obtained by splitting the pump pulse into a double-pulse sequence. With this technique it is possible to correlate the spectral response of a photoproduct, formed by the repump process during population time T, with the spectral signatures of its initially excited chemical precursors. This fifth-order approach was originally implemented in 2D infrared spectroscopy for vibrational transitions[95–98] and was later adopted by our group for electronic transitions.[99] We also note that there are further multidimensional approaches of fifth or even higher order which can address different photodynamical issues.[100–112]

Continuing this sequence of increasingly complex pulse trains, one naturally arrives at arbitrarily shaped temporal waveforms (Figure 2 g) as the most general implementation of ultrafast spectroscopy. Such pulses have been mainly employed in the realm of quantum control, where the goal is to steer quantum-mechanical wave packets along certain trajectories and/or into user-specified product states.[86,92,93,113–125] Thus, one can achieve, for example, coherent control over the outcome of chemical reactions. In the context here, shaped pulses can be interpreted as versatile spectroscopic tools for multidimensional spectroscopy, as captured by the term "quantum-control spectroscopy".[103,126]

3. Experimental Implementation

The purpose of this Review is predominantly to provide a perspective on how electronic 2D spectroscopy can be applied to unravel photochemical, rather than photophysical, ultrafast processes. These achievements go hand in hand with technological implementations such as femtosecond pulse shaping, which in turn require a description of experimental details. However, the chemical implications of the method may also be understood when jumping directly to Section 4.

3.1. Pulse Generation and Pulse Shaping

For all time-resolved measurements, 800 nm pulses of 100 fs duration at a repetition rate of 1 kHz from a regenerative amplifier system were utilized. Part of the output was used to pump a non-collinear optical parametric amplifier (NOPA) delivering tunable femtosecond pump pulses in the visible spectral range. A home-built femtosecond pulse shaper[127–130] (Figure 3) was used to compress these pulses and to precompensate the dispersion of the transient absorption setup. The pulse shaper consisted of a custom-made volume-phase-holographic (VPH) grating[131–133] with 1000 lines per mm to disperse and to recombine the spectral components of the laser pulses, and a 4f setup with a planar folding mirror, a cylindrical mirror to focus each spectral component, and a symmetry mirror. We used a programmable two-layer liquid-crystal display (LCD) with 640 pixels per

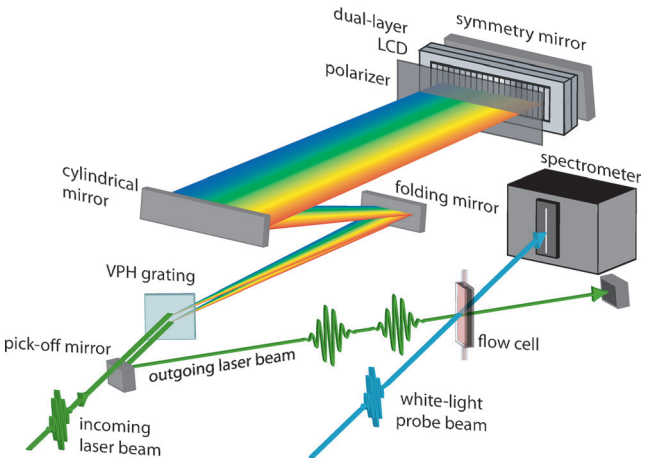

Figure 3. Experimental setup for transient absorption and multidimensional spectroscopy in pump-probe geometry. The incoming pump beam enters a femtosecond pulse shaper comprising a volume-phase-holographic (VPH) grating used to disperse the beam, a folding mirror, a cylindrical mirror, and a symmetry mirror. The pulse is manipulated in amplitude and phase using a dual-layer liquid-crystal display in combination with a linear polarizer. The symmetry mirror is slightly tilted so that the outgoing beam is displaced in the vertical direction and can be directed to the sample. The white-light probe beam and the pump beam are focused and spatially overlapped in a flow cell. The change in the absorption of the probe pulse is finally detected with a spectrometer.

layer (CRI, SLM-640) in combination with a linear polarizer to shape the laser pulses in terms of amplitude and phase.

The pulse-shaper-assisted collinear frequency-resolved optical gating (cFROG)[134,135] technique was employed to characterize and compress the pulses typically to below 25 fs duration.

3.2. Transient Absorption

For the transient absorption measurements, every second pump pulse was blocked using a phase-locked optical chopper working at 500 Hz. The white-light probe continuum was generated by focusing a small portion (< 1 μJ) of the 800 nm pulses into a continuously moving CaF_2 plate. Although sapphire is widely utilized as a stable and reliable source for a white-light continuum, the continuum generated in CaF_2 has been proven to reach further into the UV spectral range.[136–138]

A computer-controlled delay stage was used to vary the temporal delay T between the pump and probe pulses with a maximum delay of up to about 3 ns. A broadband $\lambda/2$ plate inserted in the pump beam was employed to adjust the relative polarization directions to the magic angle of 54.7° to eliminate orientational anisotropy effects in transient absorption.[139–141] Pump and probe pulses were focused and spatially overlapped in a flow cell with a path length of 200 μm. The sample was pumped through the flow cell with a microannular gear pump to refresh the pump volume between consecutive laser shots.

Behind the sample, the probe pulses are guided into a spectrometer that operates at an acquisition rate of 1 kHz and thus enables shot-to-shot detection of the probe spectrum $I(T,\bar{\nu}_{\text{probe}})$. The optical density change $\Delta\text{OD}(T,\bar{\nu}_{\text{probe}})$ caused by the pump pulse is evaluated at a rate of 500 Hz as a function of the probe wavenumber $\bar{\nu}_{\text{probe}}$ through Equation (1).

$$\Delta\text{OD}(T,\bar{\nu}_{\text{probe}}) = -lg\left[\frac{I(T,\bar{\nu}_{\text{probe}})_{\text{with pump}}}{I(\bar{\nu}_{\text{probe}})_{\text{no pump}}}\right] \quad (1)$$

White-light continua generated in transparent solid-state materials are typically strongly dispersed, thereby leading to a positive chirp of the probe pulse. This chirp can be corrected in data postprocessing[140,142] by evaluating the position of the so-called coherent artifact that is caused by nonlinear interactions between the pump and the probe pulse.[143–146] The temporal resolution of the described setup averaged over the probe axis was determined to be below 50 fs for all pump central wavelengths. All discussed measurements were performed at room temperature.

3.3. Coherent Multidimensional Spectroscopy in Pump-Probe Geometry

For the implementation of multidimensional spectroscopy to photochemical reactions we followed the approach of a partly collinear pump-probe beam geometry by splitting up the pump pulse into a double-pulse sequence. This method was first suggested by Gallagher Faeder and Jonas in 1999[147] and later implemented in the near- and mid-IR[37,148–151] and also in the visible and ultraviolet spectral range.[39,42,44,152,153]

To collect 2D spectra in a pump-probe beam geometry with a white-light probe, the change of the optical density $\Delta\text{OD}(\tau,T,\bar{\nu}_{\text{probe}})$ is measured as a function of the coherence time τ. To separate the desired 2D signal contributions (originating from a single interaction of every laser pulse with the sample) from the unwanted transient absorption background (where either pulse 1 or pulse 2 interacts twice with the sample) specific phase-cycling schemes can be applied with the pulse shaper.[151,154,155] This scheme makes use of the fact that the desired 2D signal switches its sign when the relative phase of the double pulse is changed by π, while the undesired transient absorption background is not sensitive to the relative phase. To extract the background-free 2D signal it is, therefore, sufficient to apply a two-step phase-cycling scheme by collecting the time-domain raw data twice as a function of τ with a relative phase difference of zero and π between pulses 1 and 2 and by subtracting the two data sets from each other. More flexibility, for example, for scatter removal, can be achieved by incorporating measurements with other relative phases.

To generate two identical replicas of the laser pulse, the pulse shaper mimics the spectral interference pattern which would be observed after a conventional interferometer with two separated arms. For a given coherence time τ with one pulse fixed at $t=0$, the applied spectral transfer function of the pulse shaper is given by Equation (2). [135]

$$M(\omega) = \frac{1}{2}\left[e^{-i[\omega-(1-\gamma)\omega_0]\tau}e^{-i\phi_1} + e^{-i\phi_2}\right]e^{-i\phi(\omega)_{\text{compr.}}} \quad (2)$$

Here, ω_0 is the carrier frequency of the laser pulse. The phase offset $\phi(\omega)_{\text{compr.}}$ is used to compress the laser pulses to their bandwidth limit. The phases ϕ_1 and ϕ_2 can be varied separately to conduct the above-mentioned phase-cycling schemes. The dimensionless parameter γ determines whether the carrier wave is shifted together with the pulse envelope ($\gamma=1$), just as with a mechanical interferometer, or whether only the envelope is shifted while the carrier phase remains constant ($\gamma=0$). For $\gamma=1$, the 2D signal oscillates at the transition frequency as τ is increased. The effect of γ values lower than 1 is that the phase between the pulse copies is adjusted in such a way that the apparent oscillation frequency of the desired 2D signal along τ is reduced. This approach is called the "rotating frame" and can be used to reduce the number of necessary data points along τ by extending the Nyquist limit, thereby allowing for undersampling of rapidly oscillating time-domain signals.[151,156]

Since the system is in a coherence between pulse 1 and 2 in Fourier-transform 2D spectroscopy, interferometric phase stability is required between these two pulses. The stability criteria found in the literature are typically on the order of $\lambda/100$ for fluctuations of the optical path length, which corresponds to a timing precision of 20 attoseconds for a laser pulse with a central wavelength of $\lambda=600$ nm. This is challenging to achieve with conventional non-collinear setups. Making use of frequency-domain pulse shaping in a pump-probe beam geometry solves this issue since the generated pulse copies travel along a common path and are thus inherently phase stable. Sub-attosecond precision in pulse-to-pulse delay was demonstrated using fs pulse shapers similar to ours.[157] These strict interferometric stability requirements do not apply between the (second) pump and the probe pulse (except for special cases such as double-quantum coherence 2D spectroscopy),[50–54] and the much less stringent conditions of transient absorption have to be met. For this reason, minor instabilities, for example, caused by the continuum generation, are rather uncritical for 2D spectroscopy with a continuum probe.

The absorptive 2D spectrum $S_{2D}(\bar{\nu}_{\text{pump}},T,\bar{\nu}_{\text{probe}})$ is obtained by calculating the Fourier transform of the time-domain 2D signal along τ and by taking the real part of it. Since the chirp of the probe pulse would lead to peak distortions in the 2D spectra,[158] a chirp correction is employed for the 2D data at short population times, where the chirp of the continuum cannot be neglected.[159]

In the pump-repump-probe and in the TE2D experiments a second NOPA delivered the visible pump pulses while the repump pulse was generated by taking the second harmonic of the first NOPA at 870 nm (1.15×10^4 cm^{-1}) to yield the repump pulses centered at 435 nm (2.30×10^4 cm^{-1}).

4. Molecular Systems

As stated in the introduction, we wanted to explore the applicability of multidimensional electronic spectroscopy to

photochemical, rather than purely photophysical, ultrafast processes and thus required appropriate model systems. We chose a molecular switch with various reactive channels, thus forming a "kinetic network" between reactants, intermediates, and products. The question was then whether 2D spectroscopy could discover which species were connected to each other and whether we could thereby learn something about the dynamics and reaction coordinates. For this purpose we looked for a model system with two different chemical substitution patterns such that particular reaction channels could be turned on or off at will, the idea being that we could then check if the associated cross-peaks in 2D spectroscopy appeared or disappeared, respectively. Furthermore, we wanted to perform all experiments with all the pulse sequences from Figure 2 on the same model systems to enable a systematic and comparative study of techniques.[99,160–166]

We chose the two nitro-substituted indolinobenzopyrans 6,8-dinitro-1′,3′,3′-trimethylspiro[2*H*-1-benzopyran-2,2′-indoline] (6,8-dinitro-BIPS) and 6-nitro-1′,3′,3′-trimethylspiro[2*H*-1-benzopyran-2,2′-indoline] (6-nitro-BIPS), both members of the merocyanine/spiropyran family (Figure 4a). These compounds are photochromic systems that exist in different molecular configurations with different colors, which can—depending on the solvent and the substituents—partly be interconverted by illumination with light.[167–169] As a result of these properties, these compounds have numerous potential applications ranging from optical data storage[170,171] to light-adaptive sunglasses[172] and molecular electronics,[173] or biological applications for water-soluble variants.[174–177]

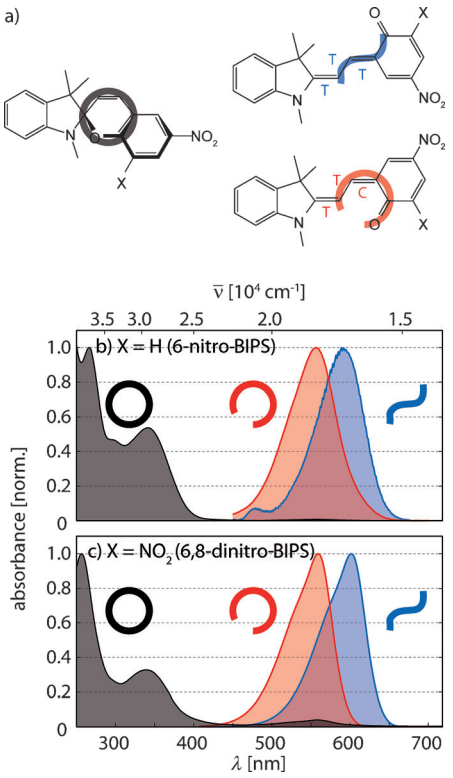

Figure 4. Model systems and linear spectra. a) The investigated indolinobenzopyrans exist either in a ring-closed spiropyran configuration (black circle) which does not absorb in the visible spectral range or as two ring-open merocyanine isomers with a *trans-trans-cis* (TTC, red open circle) or a *trans-trans-trans* configuration (TTT, blue tilde). The substituents are either X = H (6-nitro-BIPS) or X = NO_2 (6,8-dinitro-BIPS). The corresponding absorption spectra are shown for b) 6-nitro-BIPS in acetonitrile and c) 6,8-dinitro-BIPS in chloroform. Note that the UV absorption of the merocyanine isomers is not shown. The data displayed in (b) and (c) were originally discussed in Refs. [163,164] and [160,161], respectively.

The ring-closed spiropyran form (SP, closed black circle) consists of pyran and indole moieties oriented orthogonally to each other. In the investigated compounds, the pyran subunit is substituted with either one (6-nitro-BIPS, X = H) or two (6,8-dinitro-BIPS, X = NO_2) nitro groups to establish a push–pull system. As a consequence of the orthogonality of the two moieties, their π-systems do not interact, and thus the ring-closed SP does not absorb light in the visible spectral range, whereas a pronounced absorption band is observed in the UV region below 400 nm (2.50×10^4 cm^{-1}) in the case of both 6-nitro-BIPS and 6,8-dinitro-BIPS (black lines in Figure 4b,c). In contrast, the ring-open merocyanine forms (MC, blue tilde and red open circle) exhibit extended π-systems with absorption bands in the visible regime between 500 and 650 nm ($1.50–2.00 \times 10^4$ cm^{-1}, red and blue lines in Figure 4b,c). The two observed ring-open isomers differ by a *cis*/*trans* configuration in the carbon bridge that exhibits either *trans-trans-trans* (TTT: blue tilde) or *trans-trans-cis* (TTC: red open circle) geometries.

The ratio between the SP and the MC form and between the two observed MC isomers in thermal equilibrium strongly depends on the solvent and the substituents. Whereas the MC form predominates in solution for 6,8-dinitro-BIPS, the ring-closed SP is energetically favored for 6-nitro-BIPS. Since our studies focused on the photochemistry of the MC form in the visible spectral range, all 6-nitro-BIPS samples had to be illuminated with UV light during the measurements. The ratio between TTT and TTC was found to be about 1:10 at room temperature for all compounds. Both compounds (and simplified model systems) were investigated earlier by various quantum chemical[178–183] as well as time-resolved experimental[184–191] studies. Nevertheless, many aspects of their photochemistry were still unexplored before the experiments discussed in this Review.

5. Transient Absorption Spectroscopy

For the initial ultrafast experiments, the well-established transient absorption technique was employed, which provided valuable insight into the photodynamics of the system under investigation. Studies on ultrafast *cis–trans* photoisomerization generally investigate systems for which there is only one reactant isomer in solution at thermal equilibrium.[192–198] The situation was different here, in that a mixture of TTT and TTC isomers was present in solution, thereby allowing us to unravel both the forward and backward reactions at the same time and to elucidate if and how fast they occur. Transient absorption data of the investigated compounds are shown in Figure 5a–c for 6,8-dinitro-BIPS in chloroform and in Figure 5d–f for 6-nitro-BIPS in acetoni-

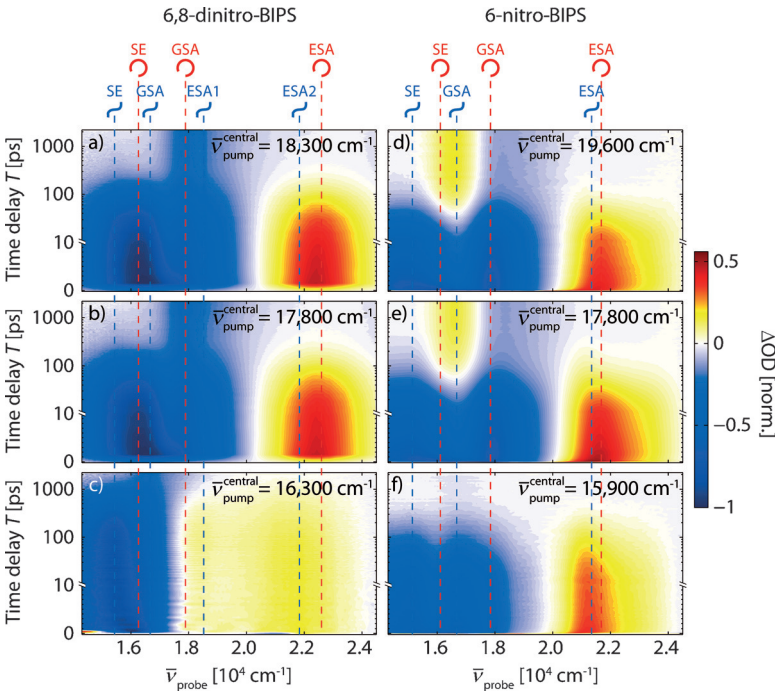

Figure 5. Transient absorption maps of a–c) 6,8-dinitro-BIPS in chloroform and d–f) 6-nitro-BIPS in acetonitrile for different pump wavenumbers. Blue/violet colors mark regions of a decreased transient absorption, while yellow/red colors indicate a pump-induced increase in absorption. The data shown in (a–c) were originally discussed in Ref. [161] and the data of (d–f) in Ref. [164].

trile. Contributions arising from an increased transient absorption (i.e. excited-state absorption, ESA, and product absorption, PA) are indicated by yellow and red colors while blue and violet colors mark regions of decreased pump-induced absorption signals (i.e. bleaching of the ground-state absorption, GSA, and stimulated emission, SE).

Since a tunable pump-pulse source was employed, the measurements could be performed with different central wavenumbers for the excitation pulses, as labeled in the upper right corner of each transient absorption map. This was done to disentangle the dynamics of the two MC isomers. Whereas excitation at the blue edge of the absorption band (Figure 5a,d) predominantly excites the TTC isomer, excitation at the red edge (Figure 5c,f) is expected to lead to a dominance of the TTT isomer (compare also the linear spectra in Figure 4b,c). ESA signals, bleaching of the GSA, and SE signals are marked in Figure 5 by red (TTC) and blue (TTT) vertical dashed lines. These contributions were assigned on the basis of a global multiexponential fit[199] to the complete data sets, and generally the signals originating from the TTT isomer are red-shifted with respect to the corresponding ones from TTC.

6,8-Dinitro-BIPS (Figure 5a–c) shows a strong ESA contribution for TTC and two ESA bands for TTT. As negative signals, bleaching of the GSA bands is observed together with SE signals that are at lower wavenumbers than the bleach of the GSA. Both the ESA and SE bands decay with characteristic S_1 lifetimes of about 95 ps for TTC and 900 ps for TTT in the solvent used. For all excitation energies, negative TTC and TTT GSA signals remain after long delay times, because both MC isomers undergo the ring-closure reaction to the SP form, which does not absorb in the visible region (black spectrum in Figure 4c) and hence does not give rise to a PA band in the visible spectral range. The associated reduced MC concentration caused by this photoreaction leads to the permanent bleaching of the MC GSA bands. From these data, the ring-closure quantum yield was estimated to be about 40% for TTC and 35% for TTT.[161]

The photochemistry of the MC forms of 6-nitro-BIPS (Figure 5d–f) differ in large parts from the behavior of their dinitro-substituted counterparts. During the first hundred picoseconds, similar contributions are detected, with the SE and ESA signals of TTT red-shifted with respect to the respective TTC signals. For larger delay times, significant differences between 6-nitro-BIPS (in acetonitrile) and 6,8-dinitro-BIPS (in chloroform) become apparent: 1) The S_1 lifetime of the two isomers is reduced to about 35 ps for TTC and about 160 ps for TTT. 2) No remaining absorption bands are visible after TTT excitation (Figure 5f), which implies that photoexcitation of this species does not result in any photoproduct. 3) TTC excitation leads to the formation of a photoproduct that absorbs in the visible region, as can be deduced from the positive PA band between 1.60 and 1.70 × 10^4 cm^{-1} emerging after 100 ps as well as from the remaining bleach of the TTC GSA.

Since the absorption wavenumber of the observed positive PA band for 6-nitro-BIPS matches the GSA wavenumber of TTT, this band can be assigned to the formation of TTT isomers in the ground state. This signature only appears after excitation at a high wavenumber where predominantly the TTC isomers absorb, so these observations can be assigned to TTC→TTT photoisomerization.[164] The quantum yield of the photoisomerization reaction in acetonitrile was determined to be (18 ± 4)%.

For a comprehensive picture of the photochemical dynamics of the molecular systems, transient absorption spectroscopy has provided the characteristic time scales of the photoinduced processes and the spectral signatures of the accessible signals. This information will thus be available for the multidimensional approaches which are closely related to the pump-probe scheme and which we use in the following to address several open questions concerning the photodynamics of the investigated systems. These open questions not answered by transient absorption are, for example, the existence of *cis–trans* isomerization for 6,8-dinitro-BIPS, which will be resolved by 2D spectroscopy in Section 7, the role of vibrational modes in photoisomerization, which is investigated with 3D spectroscopy in Section 8, the dynamics initiated upon excitation to higher electronic states, which is explored by triggered-exchange 2D spectroscopy in Section 9, and whether the relative yield of competing reaction paths

can be controlled by quantum control spectroscopy, which is discussed in Section 10.

6. From Transient Absorption to 2D Spectroscopy

Transient absorption spectroscopy is a third-order technique that provides photophysical and photochemical information along two independent axes, namely, the pump-probe time delay T and the probe wavenumber axis $\overline{\nu}_{\mathrm{probe}}$. Data sets, as presented in Figure 5, can additionally be recorded for multiple excitation wavenumbers such that they span a three-dimensional data space. This can be illustrated by stacking the transient maps along a third axis associated with the central pump wavenumber $\overline{\nu}_{\mathrm{pump}}^{\mathrm{central}}$, as visualized in Figure 6a.

Similarly, 2D spectroscopy is also a third-order method but provides spectroscopic information along the two axes $\overline{\nu}_{\mathrm{pump}}$ and $\overline{\nu}_{\mathrm{probe}}$. By recording various 2D spectra as a function of the population time T, information in the same three-dimensional spectroscopic space is provided, just as for transient absorption spectroscopy with variable excitation wavenumbers. This relation becomes apparent when the 2D spectra are stacked on top of each other along the T axis (Figure 6b).

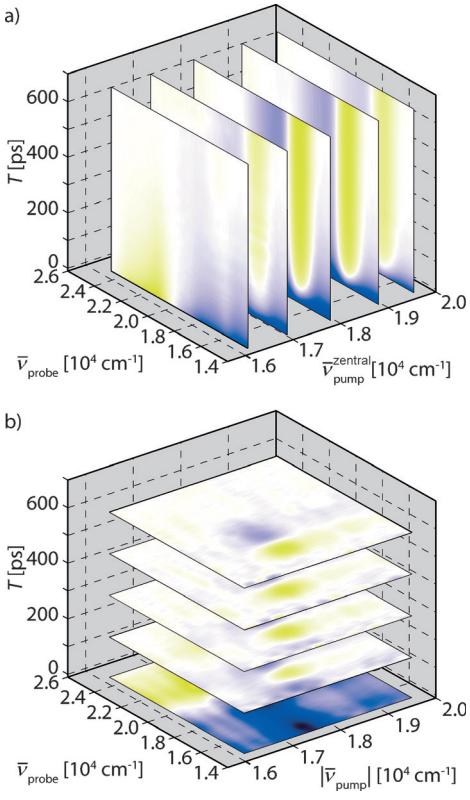

Figure 6. Relationship between transient absorption and 2D spectroscopy, visualized with the data for 6-nitro-BIPS. a) Transient absorption maps are measured with different central wavenumbers $\overline{\nu}_{\mathrm{pump}}^{\mathrm{central}}$ of the pump pulse and cover the same three-dimensional region as b) 2D spectra for various waiting times T when stacked next to each other. The data shown in (a) were originally discussed in Ref. [164] and the data of (b) in Ref. [163].

On comparing these two plots (Figure 6a,b) it is seen that the same spectral features are recovered by the two methods, that is, the blue and/or yellow signals appear at the same respective positions in the underlying 3D "data space". Thus, the question arises whether there are particular advantages to using either of the two approaches. In transient absorption, the spectral resolution along $\overline{\nu}_{\mathrm{pump}}$ is limited by the spectral bandwidth of the pump pulse and each individual transient map reflects the third-order response of the photosystem integrated over the entire pump-pulse spectrum. In coherent 2D spectroscopy, an additional laser pulse is employed and its temporal delay with respect to the first pulse—the coherence time—is scanned systematically and a Fourier transformation along τ yields the 2D spectrum. Just as in any other Fourier-transform-based method,[200] the spectral resolution is determined by the maximum delay between the first and the second pulse. Improving the resolution in regard to the pump wavenumber in transient absorption can only be achieved by narrowing the pump-pulse spectrum, which in turn will result in a lower temporal resolution as a result of the increase in the pump-pulse duration. Fourier-transform coherent 2D spectroscopy thus provides high spectral resolution while the time resolution is the same as in transient absorption.[201]

This is one of the reasons why a closer look at the two data sets shown in Figure 6a,b reveals some differences between the data measured with transient absorption and the 2D spectra, such as the positive PA band (yellow) around $\overline{\nu}_{\mathrm{probe}} = 1.70 \times 10^4\ \mathrm{cm}^{-1}$ extending to higher $\overline{\nu}_{\mathrm{pump}}$ values in Figure 6a than in Figure 6b. The first reason for differences between the data sets is that the transient-absorption data maps are measured by tuning a broadband pump laser to different central wavelengths. Even when the laser is tuned to the edge of the molecule's absorption band, the overlap of the laser spectrum with the absorption spectrum is still large enough to excite a significant amount of molecules due to the large bandwidth of the pump pulses, whose spectral edges reach further into the absorption band. Another reason is that the tuning range used to measure the data in Figure 6a is considerably broader than the single laser spectrum employed for the 2D measurements, where the spectral amplitude drops to zero at frequencies with vanishing pump spectrum.

7. 2D Spectroscopy of Photoisomerization

7.1. Schematic 2D Spectra

So far, the main field of application in the literature for 2D electronic spectroscopy has been the study of ultrafast photophysical dynamics of multichromophore systems and not single-chromophore photochemistry, as covered in this Review. Since coherent 2D spectra intuitively visualize spectral correlations in photoactive samples on femtosecond time scales, couplings between different chromophores manifest themselves in cross-peaks connecting the absorption (pump) frequency of one chromophore with the emission (probe) frequency of the respective other chromophore. A similar explanation holds if excitonic states, rather than chromophores located at a particular spatial "site" of the full

system, are used as a basis. In regard to such photophysical phenomena, 2D spectroscopy has successfully been employed to elucidate the energy-transfer processes in natural[33,36,41,42] and artificial[202,203] light-harvesting systems as well as to investigate exciton dynamics in multichromophores.[204–207] The evolution of diagonal and off-diagonal peaks in the 2D spectra as a function of waiting time reflects the properties of the energy transfer between the chromophores.

In a photochemical reaction, however, a reactant molecule transforms into another species with, for example, a different molecular configuration which is—at least on the time scale of the experiment—thermodynamically stable. The principle of coherent electronic 2D spectroscopy of reactive molecular species is sketched in Figure 7 using the example of

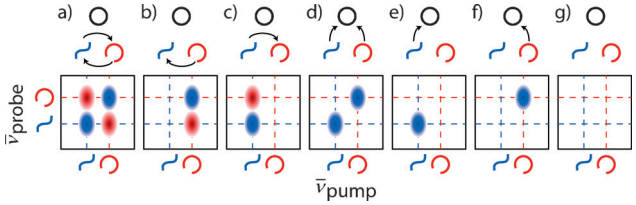

Figure 7. Potential photochemical reaction scenarios and associated 2D spectra at long population times when all molecules have relaxed to the electronic ground state, showing a) bidirectional *cis–trans* isomerization, b) unidirectional *cis-trans* and c) unidirectional *trans-cis* isomerization, d) ring closure of both MC isomers, e) ring closure of TTT, f) ring closure of TTC, and g) no photochemical reaction occurring at all. Red peaks denote photoproduct absorption signals, blue ones the associated bleach of the reactants. The symbols representing molecular configurations are in accordance with those in Figure 4a. The ring-closed form is assumed not to absorb in the spectral range covered by the two axes. Adapted from Ref. [163] with permission.

the spiropyran/merocyanine photosystem. Various reaction scenarios are shown at the top of the Figure, while the corresponding 2D spectra are illustrated below. The horizontal axis corresponds to the pump wavenumber $\bar{\nu}_{pump}$, while the vertical axis denotes the probe wavenumber $\bar{\nu}_{probe}$. In these sketches, only long waiting times are considered, that is, when photophysical excited-state dynamics are over and the system has relaxed to its (original or product) ground state.

Since our experiments are performed in the visible spectral range, only the absorption frequencies of the two MC isomers TTC (red) and TTT (blue) are considered (vertical and horizontal dashed lines), while the ring-closed spiropyran is not detectable since its main absorption band is located in the UV region. Additional peaks would appear with ultrabroadband 2D spectroscopy. In the case of a bidirectional *cis–trans* isomerization between TTC and TTT (Figure 7a), positive cross-peaks (red) would be observed at the crossings of the TTC and TTT absorption, that is, at the intersection of blue and red dashed lines. This is due to the fact that if one of the isomers is excited it will react to the corresponding other isomer where photoproduct absorption will lead to an increased 2D signal at the associated probe frequency. At the same time, the reduced ground-state absorption of the reactant will lead to negative peaks on the diagonal (blue). If only unidirectional *cis–trans* isomerization occurs (Figure 7b,c), these signatures will only be detected on the vertical line representing the absorption frequency of the reactant isomer. In Figure 7d–f the ring-closure reaction from the merocyanine isomers to spiropyran is assumed to be favored over the photoisomerization. In this case, only the negative bleaching signals corresponding to the decreased merocyanine concentration will be detected along the diagonal, since the product (the spiropyran) does not absorb in the visible spectral range. If the system under study does not undergo any photochemical reaction (Figure 7g), no signatures will be observed at all at long waiting times.

The integral of absorptive 2D spectra along the pump frequency axis yields the spectra recorded with transient absorption.[11,28,147] From this, it becomes apparent that single transient absorption measurements may yield ambiguous results, since backtracking of the photoproduct signals to its reactant is not possible because of the lack of the second (i.e. excitation) frequency axis. Furthermore, positive and negative contributions (as for example in Figure 7a) could cancel each other out in transient absorption. Thus, only 2D spectroscopy directly visualizes the correlations between reactants and products and allows for a direct and unambiguous assignment of the signatures to all involved chemical components.

Figure 7 represents a very simplified picture of the resulting 2D spectra for reactive species. Linear combinations of the sketched scenarios are possible if several reaction pathways can be followed. In practice, several further circumstances may complicate the interpretation of the measured spectra. Since electronic 2D spectroscopy involves the electronic excitation of the sample, signatures of the excited state, such as stimulated emission or excited-state absorption, dominate the 2D signal for population times on the time scale of the excited-state lifetimes of the investigated compounds. We will discuss these short-time contributions in Section 8.

7.2. Experimental 2D Spectra

Figure 8 shows the electronic 2D spectra of the merocyanine isomers of 6,8-dinitro-BIPS in chloroform at $T = 3.0$ ns (Figure 8a) and of 6-nitro-BIPS in acetonitrile at $T = 2.2$ ns (Figure 8b). The horizontal axis represents the pump wavenumber, and the vertical axis the probe wavenumber. Since a probe continuum is used in these measurements, the probe axis extends over a broader spectral range than that of the pump, whose bandwidth is limited by the NOPA. Both spectra display purely absorptive contributions and, thus, similar to the representation of the transient absorption data (Figure 5), negative values (blue) correspond to a pump-induced decreased absorption of the sample, while positive signals (yellow/red) represent an increase in the absorption. All expected contributions are marked by red (TTC) and blue (TTT) dashed lines (as in Figure 7), where the vertical lines represent the absorption frequencies of the two isomers and the horizontal lines the GSA, SE, and ESA signals as labeled.

Since the excited-state lifetimes of all the compounds are below 1 ns, these 2D spectra reflect the net photochemical

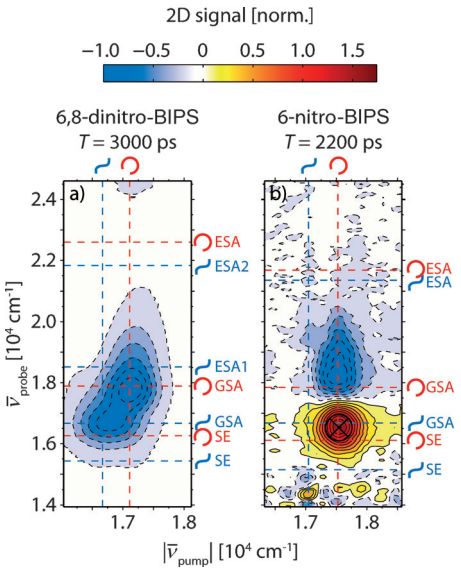

Figure 8. 2D spectra for long waiting times. The sign convention is similar to the representation of the transient absorption data. In addition, dashed contour lines are used for negative parts of the spectrum, while solid contour lines mark positive regions. a) The 2D spectrum of 6,8-dinitro-BIPS at $T = 3000$ ps indicates that both MC isomers undergo the ring-closure reaction to the spiropyran form. b) A positive cross-peak in the 2D spectrum of 6-nitro-BIPS at $T = 2200$ ps proves the existence of the unidirectional TTC→TTT photoisomerization reaction. Figure (a) adapted with permission from Ref. [162]. Copyright American Chemical Society (2011). Figure (b) adapted from Ref. [163] with permission.

change after the deactivation of all the excited states is completed. Therefore, these 2D spectra may directly be compared to the scenarios discussed in Figure 7. In the 2D spectrum of 6,8-dinitro-BIPS (Figure 8a), two slightly overlapping negative signals are observed at the TTC excitation/TTC GSA probe and TTT excitation/TTT GSA probe wavenumbers. These two peaks arise from the permanent bleaching of the two MC isomers and the best agreement is found with the sketched 2D spectrum of Figure 7d, where the ring closure of the two MC isomers is favored over *cis–trans* isomerization. Since no positive cross-peaks are found, the *cis–trans* isomerization can be excluded as a major reaction path for this compound. The 2D spectrum of 6-nitro-BIPS (Figure 8b) considerably differs from that of its dinitro-substituted version. A positive cross-peak is found at TTC excitation and TTT GSA probe wavenumbers (circled black cross) together with a negative contribution at TTC GSA probe wavenumbers. In agreement with the sketch from Figure 7b, this finding indicates the existence of TTC→TTT photoisomerization while no signal is observed for TTT excitation. This directly proves that the *cis-trans* isomerization is favored over any other photoreaction for 6-nitro-BIPS, but only for one of the two ring-open isomers (TTC), while the other isomer (TTT) decays back to its electronic ground state without undergoing any photochemical change.

8. Third-Order 3D Spectroscopy

The 2D spectrum shown in Figure 8b represents only the permanent chemical changes observed for 6-nitro-BIPS after photoexcitation. However, we wish to gain a more comprehensive picture and also retrieve information about the reaction mechanism, namely, the short-time dynamics on the reactive potential-energy surface. For this purpose we recorded 2D spectra for a large number of population times T (similar as in Figure 6b, but in many small time steps). Figure 9 shows a cut through this data set along T at the spectral position of the positive cross-peak marked by the black cross in Figure 8b. The positive cross-peak emerges for population times larger than about 100 ps (see the data point marked by the black cross that corresponds to Figure 8b). For shorter times, the 2D signal is negative in this region. The excited-state lifetime of the TTC isomer of 6-nitro-BIPS is about 35 ps, and so the 2D spectrum is dominated for $T <$ 100 ps by SE and bleaching of the GSA band. Both SE and GSA bleach give rise to negative 2D signals, which, however, are centered at different positions in the 2D spectra. The most prominent feature of the cross-peak signal of Figure 9 is the occurrence of pronounced oscillations for population times below 1.5 ps. These oscillations can be attributed to coherent vibrational wave-packet motion induced by the broadband excitation with femtosecond laser pulses.

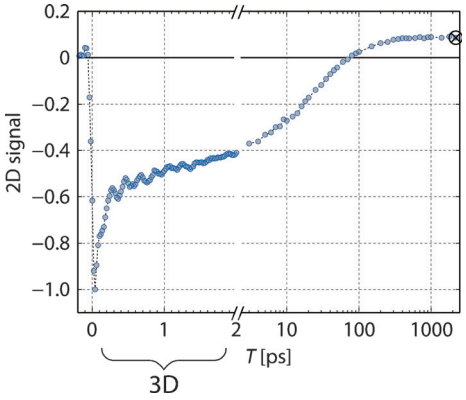

Figure 9. A cut through the 2D data of 6-nitro-BIPS along T at the spectral position of the positive cross-peak reveals coherent vibrational wave-packet dynamics up to 2 ps after excitation. The 2D data for $T < 2$ ps is the source for the third-order 3D spectrum presented in Figure 10. The cross marks the data point labeled in Figure 8. The data were originally discussed in Ref. [163].

To decipher the connection of these molecular vibrations to the chemical reaction, a third-order three-dimensional (3D) spectrum is generated by applying a Fourier transformation of the 2D data set along T (for $0 < T < 2$ ps as indicated in Figure 9), thereby yielding a third wavenumber axis $\bar{\nu}_T$.[163] This additional axis is now associated with the frequency of coherent oscillations between the pump sequence and the probe pulse and unravels the complex time-domain data by separating the non-oscillating portion of the signal from the oscillating signatures.

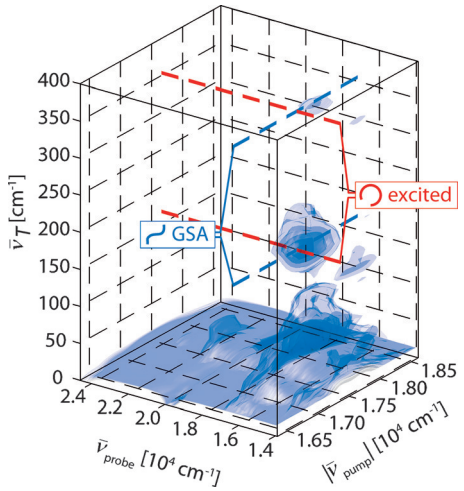

Figure 10. Third-order 3D spectrum of 6-nitro-BIPS in acetonitrile represented by four different isosurfaces at values of 0.65%, 0.9%, 1.15%, and 1.40% of the maximum. The red dashed lines mark the TTC excitation wavenumber, while the blue dashed lines indicate the GSA probe wavenumber of the TTT isomer. Two 3D cross-peaks are observed, thus indicating that two independent vibrational modes are involved in the photoisomerization reaction. Figure adapted from Ref. [163] with permission.

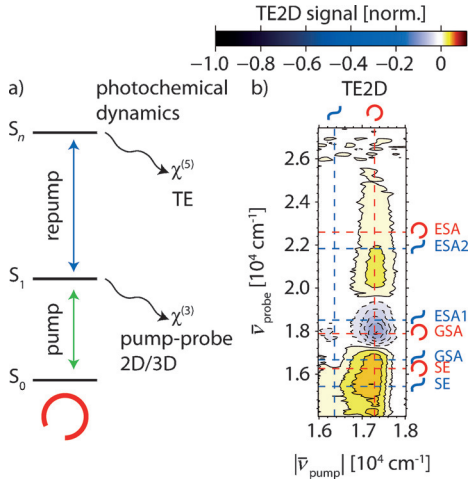

Figure 11. Triggered-exchange 2D (TE2D) spectroscopy of 6,8-dinitro-BIPS. a) A pump pulse in the visible region is used to excite the molecule to its first excited electronic state S_1. Third-order techniques, such as pump-probe/transient absorption or coherent 2D/3D spectroscopy, can be used to monitor the dynamics emanating from this S_1 population. By using an additional repump pulse resonant with the S_1-S_n excited-state absorption at 435 nm, a part of the S_1 population is transferred to a higher-lying electronic state and fifth-order TE2D is used to observe the photochemical dynamics originating from the repump process. b) TE2D spectrum of 6,8-dinitro-BIPS in chloroform for $t_{PR} = 0.5$ ps and $T = 2000$ ps. Figure (b) adapted from Ref. [99] with permission. Copyright American Physical Society (2013).

The resulting third-order 3D spectrum is shown in Figure 10 using an isosurface representation. The wavepacket oscillations cause two separated 3D cross-peaks located at $\bar{\nu}_T = 176$ and 363 cm^{-1}, thereby showing that two independent vibrational modes are involved in the observed photodynamics with oscillation periods of about 190 and 90 fs, respectively. Furthermore, by taking the position of these cross-peaks in the $(\bar{\nu}_{pump}, \bar{\nu}_{probe})$ plane into account, it becomes apparent that both modes are involved in the *cis–trans* isomerization since they are both located at TTC excitation (red dashed lines) and TTT GSA (blue dashed lines) wavenumbers connecting the absorption frequency of the reactant with the absorption frequency of the product. Further investigations showed that the wave packet is finally observed in the first excited electronic state S_1 of the TTT isomer,[163] which means that vibrational coherence is maintained during the torsional motion of the molecule necessary for photoisomerization. The product is, thus, formed in the electronically excited state and afterwards relaxes down to the electronic ground state. The final relaxed product gives rise to the positive absorption features detected in transient absorption (Figure 5d) and 2D measurements (Figure 8b) for large T values.

9. Triggered-Exchange 2D Electronic Spectroscopy

In all the experiments discussed so far, the photoreactions were investigated after a single excitation to the first electronically excited state. As sketched in Figure 11a (green arrow), pump-probe, 2D and third-order 3D spectroscopy provide us with detailed insights into the photochemistry after excitation to S_1. Since the observed signals arise after two interactions with the electric field of the pump pulse (or in the case of 2D spectroscopy, with the pump-pulse pair) and a third interaction with the probe pulse, the total number of three interactions makes these techniques third-order spectroscopy methods that probe the third-order nonlinear susceptibility tensor $\chi^{(3)}$ (see also Figure 2b–d).

We now proceed to retrieve information on photochemical channels from higher-lying electronically excited states. For this purpose, additional light–matter interactions are introduced (Figure 11a, blue arrow). This was done by using a pump pulse to excite 6,8-dinitro-BIPS in the visible spectral range and applying an additional repump pulse, delayed by the pump-repump time delay t_{PR} and resonant to the excited-state absorption around 435 nm to induce the $S_1 \rightarrow S_n$ transition (see also pulse sequence in Figure 2e). The experiments disclosed that a new photoproduct is formed,[99] which shows a broad absorption band in the visible spectral range. Since both merocyanine isomers exhibit excited-state absorptions in the spectral range of the repump pulse, an assignment of the observed product to its precursor isomer is not straightforward on the basis of pump-repump-probe measurements. For this reason, we implemented coherent triggered-exchange two-dimensional (TE2D) electronic spectroscopy, which is basically a combination of the conventional 2D spectroscopy with pump-repump-probe spectroscopy. The pump pulse was again split into a double-pulse sequence with pulse separation τ (see Figure 2f) using our femtosecond pulse shaper, and a separate repump laser pulse was applied. 2D spectra at fixed pump-repump delays and population times were recorded.

The extracted TE2D spectrum for $t_{PR} = 0.5$ ps and $T = 2000$ ps is shown in Figure 11b. This TE2D spectrum can be

regarded as the change in the conventional electronic 2D spectrum with excitation to S_1 as a result of the additional interaction of the excited-state population with the repump pulse. In this way, we can access the correlation between the initially excited isomer and the spectral signatures of the species formed by repumping. This signature consists of a broad positive photoproduct absorption which is superposed by a corresponding bleaching of the merocyanine ground state. Similar features have been observed for other merocyanines[208] and are assigned to the merocyanine radical cation formed upon absorption of both a pump and repump photon. The TE2D approach allows the TTC isomer to be unambiguously identified as the precursor isomer of the radical cation, since its signatures are located at TTC excitation wavenumbers (vertical red dashed line). In contrast, no additional reaction path after $S_1 \rightarrow S_n$ repumping is identified for the TTT isomer of 6,8-dinitro-BIPS because no signal emerges at the vertical blue dashed line in Figure 11b. Thus, TE2D spectroscopy revealed that only one of the isomers forms a radical cation after excitation to higher-lying electronic states by consecutive absorption of two photons.

10. Quantum-Control Spectroscopy

Although femtosecond transient absorption, coherent 2D/3D spectroscopy, and their discussed extensions can be used to observe photodynamical processes of a given nonlinearity with very high temporal resolution, the investigation of these processes can be further generalized by applying intense, structured femtosecond pulses. On the one hand, the temporal moments at which the system interacts with such shaped pulses can be distributed in a versatile way, with one pulse comprising several possibilities for a sequence of interactions. On the other hand, higher nonlinearities can be addressed and processes of different nonlinearity can be investigated concurrently. Imagine a system for which several photochemical reaction paths are possible, but additional repump steps are required for some of them. Restricting the probed signal to a certain nonlinearity will not disclose all of these reaction paths. This is already true for our model systems, where formation of a radical cation with visible light necessitates a repumping step (as revealed by the fifth-order TE2D technique), but competes with processes of lower nonlinearity that can follow an excitation by the pump pulse, such as ring closure, *cis–trans* isomerization, fluorescence, and internal conversion. Hence, we conducted quantum control experiments with shaped femtosecond pulses as an extension to the foregoing spectroscopic studies to explore the initial steps in the isomerizing 6-nitro-BIPS merocyanine.[166] We specifically tackled the question of which fraction of all the excited molecules proceeds along a particular reaction pathway and what is the time scale on which a putative bifurcation is passed.

The existence of competing photoreactions for the merocyanine form of 6-nitro-BIPS is revealed in excitation-power-dependent measurements, where the formation of the radical cation is found at high pulse energies, as already observed for 6,8-dinitro-BIPS in the TE2D measurements (see Section 9). Thus, in the high-power-excitation regime the resonant two-photon radical cation formation can be initiated with one and the same laser pulse, successively triggering the pump as well as the repump transition. In this way, three competing reaction channels—one-photon isomerization, one-photon relaxation, and two-photon radical cation formation—arise under certain conditions.

To investigate the fraction of molecules associated with a reaction channel, we varied the linear chirp of the excitation pulse under high-power conditions. The linear chirp of the laser pulse has been used successfully as a major control parameter in the field of quantum control and spectroscopy in numerous time-resolved studies.[117,209–220] In our experiment, this was done by applying a second-order spectral phase centered around frequency ω_0 to the pump pulse [Eq. (3)].

$$\Phi(\omega) = \frac{1}{2}\Phi''(\omega)(\omega - \omega_0)^2 \tag{3}$$

The second-order dispersion $\Phi''(\omega)$ was systematically scanned using our femtosecond pulse shaper. For positive Φ'' values, lower frequencies temporally precede the higher frequency components, and vice versa for negative Φ'' values.

Intrapulse pump-dump processes dominate in the raw data (not shown). This effect was first predicted in 1990[221] and later observed in high-power experiments on molecules in solution.[196,210,213,219,222–226] Negatively chirped pulses efficiently dump the population back to the electronic ground state through stimulated emission, since the instantaneous frequency of the pulse matches the shrinking energy gap between the excited-state population relaxing away from the Franck–Condon region towards lower-lying areas of the S_1 potential energy surface and the ground state. This intrapulse pump-dump effect is suppressed for positively chirped pulses, since the increasing instantaneous frequency of the pulse is opposite to the transition frequency required for the population back transfer. Thus positive chirp results in an increase in the remaining excited-state population.

The effect of this well-known process can be removed by normalizing the data to the amount of molecules remaining in the excited state after the pump pulse. This was done by collecting transient absorption spectra at $T = 2$ ns and dividing these spectra by the amplitude of the bleached GSA signal recorded at $T = 8$ ps. The absolute quantum yield of each reaction channel was then estimated on the basis of a spectral fitting model.[166] The resulting chirp dependence of the individual quantum yields is shown in Figure 12 for all three reaction paths. Both the relaxation (Figure 12a) and the photoisomerization (Figure 12b) quantum yields show a distinct minimum at slightly negative chirp values of $\Phi''(\omega) = -200$ fs^2 and an increase for more negative and for positive dispersion values. The reason for this behavior can be seen in Figure 12c, which depicts the ionization quantum yield as a function of the linear chirp. Since this graph is the mirror image of the other two graphs, we can conclude that the quantum yields of both the isomerization and the relaxation channels are determined by the amount of ionization that serves as a "loss channel" for the other reaction paths. The shape of the curve in Figure 12c can be explained by the resonant nature of the two-photon ionization, for which the

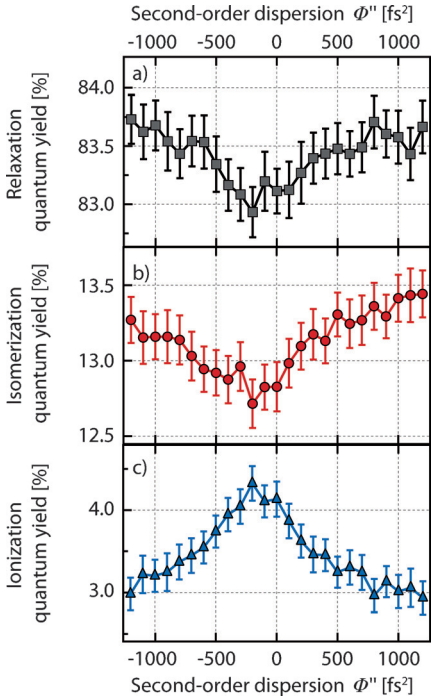

Figure 12. Quantum-control spectroscopy of competing reaction channels. Under high-power-excitation conditions the ratio of the quantum yields of the three reaction channels (a) relaxation, (b) photoisomerization, and (c) resonant two-photon ionization of 6-nitro-BIPS is controlled by varying the linear chirp of the excitation pulse. Figure adapted from Ref. [166] with permission. Copyright American Chemical Society (2014).

transient dynamics of the wave packet on the S_1 potential have to be taken into account. The intrapulse pump-repump process (to the ionization state) is optimal when the ordering of the spectral excitation components fits to the time evolution of the energy gap between the S_1 wave packet and the S_n potential energy surface. Thus, a particular negative chirp value is optimal for ionization. In contrast, the maximum ionization yield in the case of a nonresonant two-photon process would be expected for unchirped pulses, for which the pulse's peak intensity is maximal.

The discussed data provides useful information on the involved potential energy surfaces and the reaction dynamics. From the optimal $\Phi''(\omega)$ value for the formation of a radical cation we can deduce that the minimum of the S_n potential is shifted along the reaction coordinate in the same direction with respect to the S_1 as the S_1 minimum is shifted compared to the S_0 equilibrium configuration. Furthermore, the small chirp value necessary for optimal reexcitation to S_n implies a very fast initial motion of the S_1 wave packet towards lower-lying regions of the S_1 potential. This in turn suggests that the excited-state isomerization is also very fast. From the position of the extrema in Figure 12, one can deduce that the decision which reaction path is followed is not determined instantly. Hence, a molecule which started the isomerization can still be ionized on a timescale of 100 fs or longer. Quantum-control spectroscopy thus demonstrates that the excited-state isomerization reaction is an ultrafast process, with the initial excitation and the subsequent well-timed provision of a further photon being the decisive steps determining the quantum yields of the three competing reaction channels.

11. Conclusion

Each of the discussed experimental approaches provides another piece of the puzzle and together lead to a detailed and comprehensive picture about the photochemical reaction network under study. The main results are summarized in Figure 13 for the merocyanine isomers of 6-nitro-BIPS by making use of two major reaction coordinates: a generalized vibrational coordinate (red) and the torsional coordinate (blue) describing the *cis–trans* isomerization between the merocyanine isomers. After absorption of a photon in the visible range, the major part of the excited TTC molecules relaxes back to the electronic ground state. Pump–dump processes are observed under high-energy excitation conditions. The absorption of a second photon opens up a new reaction path to the radical cation of the TTC isomer, which is formed in higher excited electronic states. About 18% of the excited TTC isomers undergo an ultrafast excited-state *cis–trans* photoisomerization from the TTC to the TTT isomer, with pronounced vibrational wave-packet motion being observed. The data shows that both radical cation formation and *trans–cis* photoisomerization can be excluded as a major reaction path for the TTT isomer.

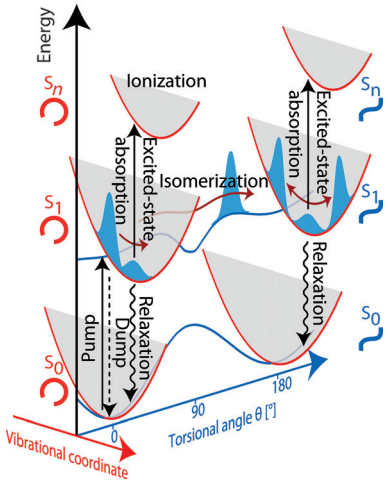

Figure 13. Reaction scheme of the TTC merocyanine isomer of 6-nitro-BIPS summarizing the results of the presented time-resolved experiments. After excitation in the visible regime, the major part of the excited molecules relaxes back to the electronic ground state through fluorescence. We also observed intrapulse dumping to the ground state and resonant two-photon ionization resulting in the radical cation formation of the TTC isomer in pump-repump-probe and TE2D measurements and under high-power excitation. A minor part of the excited molecules undergoes an excited-state *cis–trans* photoisomerization reaction along the torsional coordinate (blue) to the TTT isomer. Pronounced wave-packet oscillations were observed in the direction of a vibrational nuclear coordinate (red). The isomerization reaction is followed by fluorescence to the electronic ground state of TTT. Figure adapted from Refs. [163] and [166] with permission. Copyright American Chemical Society (2014).

This Review has outlined the suitability of coherent electronic multidimensional spectroscopy for the study of photochemical reactions. We have followed a systematic approach of increasingly complex pulse sequences and applied all techniques to the same prototype molecular system. Whereas transient absorption provides valuable information on reaction time scales and spectroscopic signatures of reaction intermediates and products, clarity on which reactant actually turns into which product molecule is gained in an intuitive way from coherent 2D electronic spectra. Further insight into the reaction pathways accessible after the initial excitation can be obtained by expansion of the 2D spectroscopy scheme. Whether coherent vibrational motion is generally induced after excitation or might be associated with a certain photochemical process can be explored by third-order 3D electronic spectroscopy, because it directly visualizes whether this vibration connects a reactant with a specific product. The impact of further excitation of already excited molecules and newly generated photoproducts are obtained in triggered-exchange 2D electronic spectroscopy. Although providing a further photon to a proceeding photochemical reaction sequence can be a means to manipulate the reaction outcome, TE2D spectroscopy can help to elucidate which intermediate originating from which reactant takes up the photon energy. Since the connection between reactant and final product molecule is preserved in all of the multidimensional approaches, the course of different photochemical reaction pathways is obtainable without ambiguities. With quantum-control spectroscopy, information on the relative population distribution corresponding to reaction channels accessible with a different number of photons is obtained within the same experiment, thereby providing further insight into the underlying reaction mechanisms.

Although highly popular and applied to a variety of relevant questions in time-resolved spectroscopy, electronic 2D spectroscopy faces a considerable number of technical challenges. Currently, the limiting factors of electronic 2D spectroscopy, partly also in regard to the presented experimental setup, are phase stability, limited spectral bandwidths of the pump pulses, the accessible spectral regime, data acquisition time, and the signal-to-noise ratio. The issues connected with the phase stability were solved here using frequency-domain pulse shaping and by making use of a partly collinear pump-probe beam geometry. Actively[227,228] and passively[30–32,38,223–232] stabilized experimental arrangements have been developed for setups with conventional optics. Extending the limited spectral bandwidth of the pump pulses is currently one of the most frequently addressed questions in electronic multidimensional spectroscopy. A small number of promising studies involving ultrabroadband laser pulses, for example, generated by filamentation in gases or by using hollow-core fibers, have been published recently.[233–237] Extending the accessible spectral range, for example, into the near and deep UV, has also been one of the main efforts of scientists working in this field, which has countless potential applications.[39,40,43,44,238] Many different methods exist to reduce the data acquisition time and to increase the signal-to-noise ratio. Shot-to-shot pulse shaping,[152,153] shot-to-shot mechanical chopping and detection combined with high-repetition-rate laser systems,[229,232,239,240] and single-shot techniques[241,242] are currently the most efficient approaches. A more detailed discussion of experimental implementations and associated challenges has recently been elaborated by the Ogilvie group.[16]

When a molecular system exhibits multifaceted photochemistry, the spectroscopic techniques to elucidate it have to be very versatile as well to capture the many processes that can be induced by light. Our studies have demonstrated this exemplarily for merocyanine/spiropyran systems and corroborate in an illustrative fashion that whenever ambiguities remain with a certain spectroscopic method, an extension to a more advanced approach can be highly beneficial for further insight. Prospective photochemical issues to be addressed in future studies are, for example, concurrent reaction sequences, isomer-selective reactions, the generation and subsequent reaction of intermediate ions, radicals, and spin multiplet systems, or light-triggered exchange reactions.

The field of "femtochemistry" has seen tremendous development since the first ultrafast pump-probe experiments on molecular wave-packet dynamics and photodissociation reactions. The concept of multidimensional spectroscopy opens up many further avenues of research.

Acknowledgements

We are thankful to all our collaborators who contributed to the research outlined in this Review, in particular Dr. Johannes Buback, Dr. Cristina Consani, Meike Diekmann, Prof. Dr. Bernd Engels, Dr. Martin Kullmann, Dr. Florian Langhojer, Dr. Ralf Schmidt, Christof Walter, and Prof. Dr. Frank Würthner. Funding from the Bavarian research network "Solar Technologies Go Hybrid" and from the DFG (Deutsche Forschungsgemeinschaft) within the Research Unit "Light-Induced Dynamics in Molecular Aggregates" (FOR 1809) is gratefully acknowledged. P.N. further thanks the DFG for support within the Emmy-Noether program and the Cluster of Excellence RESOLV (EXC 1069).

How to cite: *Angew. Chem. Int. Ed.* **2015**, *54*, 11368–11386
Angew. Chem. **2015**, *127*, 11526–11546

[1] W. P. Aue, E. Bartholdi, R. R. Ernst, *J. Chem. Phys.* **1976**, *64*, 2229–2246.
[2] G. E. Martin, *Two-dimensional NMR methods for establishing molecular connectivity*, VCH, New York, **1988**.
[3] R. R. Ernst, *Principles of nuclear magnetic resonance in one and two dimensions*, Clarendon, Oxford, **2004**.
[4] C. P. Poole, *Electron Spin Resonance, A Comprehensive Treatise on Experimental Techniques, 2nd ed.*, Dover, Mineola, **1996**.
[5] S. K. Misra, *Multifrequency Electron Paramagnetic Resonance: Theory and Applications, 1st ed.*, Wiley VCH, Weinheim, **2011**.
[6] S. Mukamel, *Principles of Nonlinear Optical Spectroscopy*, Oxford University Press, New York, **1995**.
[7] M. Cho, *Two-Dimensional Optical Spectroscopy*, CRC, Boca Raton, **2009**.
[8] P. Hamm, M. Zanni, *Concepts and Methods of 2D Infrared Spectroscopy*, Cambridge University Press, New York, *1st ed.*, **2011**.

[9] M. D. Fayer, *Ultrafast Infrared Vibrational Spectroscopy*, CRC, Boca Raton, **2013**.
[10] S. Mukamel, *Annu. Rev. Phys. Chem.* **2000**, *51*, 691 – 729.
[11] D. M. Jonas, *Annu. Rev. Phys. Chem.* **2003**, *54*, 425 – 463.
[12] R. M. Hochstrasser, *Proc. Natl. Acad. Sci. USA* **2007**, *104*, 14190 – 14196.
[13] M. Cho, *Chem. Rev.* **2008**, *108*, 1331 – 1418.
[14] S. T. Cundiff, S. Mukamel, *Phys. Today* **2013**, *66*, 44 – 49.
[15] J. P. Ogilvie, K. J. Kubarych, *Adv. At. Mol. Opt. Phys.* **2009**, *57*, 249 – 321.
[16] F. D. Fuller, J. P. Ogilvie, *Annu. Rev. Phys. Chem.* **2015**, *66*, 667 – 690.
[17] M. T. Zanni, R. M. Hochstrasser, *Curr. Opin. Struct. Biol.* **2001**, *11*, 516 – 522.
[18] M. Khalil, N. Demirdöven, A. Tokmakoff, *J. Phys. Chem. A* **2003**, *107*, 5258 – 5279.
[19] M. Cowan, B. Bruner, N. Huse, J. Dwyer, B. Chugh, E. Nibbering, T. Elsaesser, R. Miller, *Nature* **2005**, *434*, 199 – 202.
[20] S. Park, K. Kwak, M. D. Fayer, *Laser Phys. Lett.* **2007**, *4*, 704.
[21] J. F. Cahoon, K. R. Sawyer, J. P. Schlegel, C. B. Harris, *Science* **2008**, *319*, 1820 – 1823.
[22] P. Hamm, J. Helbing, J. Bredenbeck, *Annu. Rev. Phys. Chem.* **2008**, *59*, 291 – 317.
[23] N. T. Hunt, *Chem. Soc. Rev.* **2009**, *38*, 1837 – 1848.
[24] M. Fayer, *Annu. Rev. Phys. Chem.* **2009**, *60*, 21 – 38.
[25] S. Park, M. Ji, *ChemPhysChem* **2011**, *12*, 799 – 805.
[26] D. Czurlok, J. Torres-Alacan, P. Vöhringer, *J. Chem. Phys.* **2015**, *142*, 212402.
[27] J. D. Hybl, A. W. Albrecht, S. M. G. Faeder, D. M. Jonas, *Chem. Phys. Lett.* **1998**, *297*, 307 – 313.
[28] J. D. Hybl, A. A. Ferro, D. M. Jonas, *J. Chem. Phys.* **2001**, *115*, 6606.
[29] P. Tian, D. Keusters, Y. Suzaki, W. S. Warren, *Science* **2003**, *300*, 1553 – 1555.
[30] T. Brixner, T. Mančal, I. V. Stiopkin, G. R. Fleming, *J. Chem. Phys.* **2004**, *121*, 4221 – 4236.
[31] T. Brixner, I. V. Stiopkin, G. R. Fleming, *Opt. Lett.* **2004**, *29*, 884 – 886.
[32] M. L. Cowan, J. P. Ogilvie, R. J. D. Miller, *Chem. Phys. Lett.* **2004**, *386*, 184 – 189.
[33] T. Brixner, J. Stenger, H. M. Vaswani, M. Cho, R. E. Blankenship, G. R. Fleming, *Nature* **2005**, *434*, 625 – 628.
[34] P. F. Tekavec, G. A. Lott, A. H. Marcus, *J. Chem. Phys.* **2007**, *127*, 214307 – D21.
[35] D. Zigmantas, E. L. Read, T. Mančal, T. Brixner, A. T. Gardiner, R. J. Cogdell, G. R. Fleming, *Proc. Natl. Acad. Sci. USA* **2006**, *103*, 12672 – 12677.
[36] G. S. Engel, T. R. Calhoun, E. L. Read, T. Ahn, T. Mancal, Y. Cheng, R. E. Blankenship, G. R. Fleming, *Nature* **2007**, *446*, 782 – 786.
[37] E. M. Grumstrup, S. Shim, M. A. Montgomery, N. H. Damrauer, M. T. Zanni, *Opt. Express* **2007**, *15*, 16681 – 16689.
[38] U. Selig, F. Langhojer, F. Dimler, T. Löhrig, C. Schwarz, B. Gieseking, T. Brixner, *Opt. Lett.* **2008**, *33*, 2851 – 2853.
[39] C. Tseng, S. Matsika, T. C. Weinacht, *Opt. Express* **2009**, *17*, 18788 – 18793.
[40] U. Selig, C. Schleussner, M. Foerster, F. Langhojer, P. Nuernberger, T. Brixner, *Opt. Lett.* **2010**, *35*, 4178 – 4180.
[41] E. Collini, C. Y. Wong, K. E. Wilk, P. M. G. Curmi, P. Brumer, G. D. Scholes, *Nature* **2010**, *463*, 644 – 647.
[42] J. A. Myers, K. L. M. Lewis, F. D. Fuller, P. F. Tekavec, C. F. Yocum, J. P. Ogilvie, *J. Phys. Chem. Lett.* **2010**, *1*, 2774 – 2780.
[43] B. A. West, A. M. Moran, *J. Phys. Chem. Lett.* **2012**, *3*, 2575 – 2581.
[44] N. Krebs, I. Pugliesi, J. Hauer, E. Riedle, *New J. Phys.* **2013**, *15*, 085016.
[45] C. Consani, G. Auböck, F. van Mourik, M. Chergui, *Science* **2013**, *339*, 1586 – 1589.
[46] F. V. A. Camargo, H. L. Anderson, S. R. Meech, I. A. Heisler, *J. Phys. Chem. A* **2015**, *119*, 95 – 101.
[47] G. R. Fleming, *Chemical Applications of Ultrafast Spectroscopy*, *Vol. 13*, Oxford University Press, New York, **1986**.
[48] J. D. Simon, *Ultrafast Dynamics of Chemical Systems*, Kluwer, Dordrecht, **1994**.
[49] A. H. Zewail, *Femtochemistry*: *Ultrafast Dynamics of the Chemical Bond*, World Scientific, Singapore, **1994**.
[50] D. Abramavicius, D. V. Voronine, S. Mukamel, *Proc. Natl. Acad. Sci. USA* **2008**, *105*, 8525 – 8530.
[51] K. Stone, K. Gundogdu, D. Turner, X. Li, S. Cundiff, K. Nelson, *Science* **2009**, *324*, 1169 – 1173.
[52] J. Kim, S. Mukamel, G. D. Scholes, *Acc. Chem. Res.* **2009**, *42*, 1375 – 1384.
[53] E. C. Fulmer, P. Mukherjee, A. T. Krummel, M. T. Zanni, *J. Chem. Phys.* **2004**, *120*, 8067 – 8078.
[54] N. Christensson, F. Milota, A. Nemeth, I. Pugliesi, E. Riedle, J. Sperling, T. Pullerits, H. F. Kauffmann, J. Hauer, *J. Phys. Chem. Lett.* **2010**, *1*, 3366 – 3370.
[55] D. B. Turner, K. W. Stone, K. Gundogdu, K. A. Nelson, *J. Chem. Phys.* **2009**, *131*, 144510.
[56] P. Nuernberger, K. F. Lee, M. Joffre, *Acc. Chem. Res.* **2009**, *42*, 1433 – 1441.
[57] J. A. Davis, C. R. Hall, L. V. Dao, K. A. Nugent, H. M. Quiney, H. H. Tan, C. Jagadish, *J. Chem. Phys.* **2011**, *135*, 044510.
[58] D. Hayes, G. S. Engel, *Biophys. J.* **2011**, *100*, 2043 – 2052.
[59] H. Li, A. D. Bristow, M. E. Siemens, G. Moody, S. T. Cundiff, *Nat. Commun.* **2013**, *4*, 1390.
[60] S. T. Cundiff, *Phys. Chem. Chem. Phys.* **2014**, *16*, 8193 – 8200.
[61] D. B. Turner, R. Dinshaw, K. Lee, M. S. Belsley, K. E. Wilk, P. M. G. Curmi, G. D. Scholes, *Phys. Chem. Chem. Phys.* **2012**, *14*, 4857 – 4874.
[62] T. R. Calhoun, N. S. Ginsberg, G. S. Schlau-Cohen, Y. Cheng, M. Ballottari, R. Bassi, G. R. Fleming, *J. Phys. Chem. B* **2009**, *113*, 16291 – 16295.
[63] G. Panitchayangkoon, D. Hayes, K. A. Fransted, J. R. Caram, E. Harel, J. Wen, R. E. Blankenship, G. S. Engel, *Proc. Natl. Acad. Sci. USA* **2010**, *107*, 12766 – 12770.
[64] N. Christensson, F. Milota, J. Hauer, J. Sperling, O. Bixner, A. Nemeth, H. F. Kauffmann, *J. Phys. Chem. B* **2011**, *115*, 5383 – 5391.
[65] D. B. Turner, K. E. Wilk, P. M. G. Curmi, G. D. Scholes, *J. Phys. Chem. Lett.* **2011**, *2*, 1904 – 1911.
[66] V. Butkus, D. Zigmantas, L. Valkunas, D. Abramavicius, *Chem. Phys. Lett.* **2012**, *545*, 40 – 43.
[67] N. Christensson, H. F. Kauffmann, T. Pullerits, T. Mancal, *J. Phys. Chem. B* **2012**, *116*, 7449 – 7454.
[68] G. S. Schlau-Cohen, A. Ishizaki, T. R. Calhoun, N. S. Ginsberg, M. Ballottari, R. Bassi, G. R. Fleming, *Nat. Chem.* **2012**, *4*, 389 – 395.
[69] S. Westenhoff, D. Palecek, P. Edlund, P. Smith, D. Zigmantas, *J. Am. Chem. Soc.* **2012**, *134*, 16484 – 16487.
[70] C. Kreisbeck, T. Kramer, *J. Phys. Chem. Lett.* **2012**, *3*, 2828 – 2833.
[71] C. Kreisbeck, T. Kramer, A. Aspuru-Guzik, *J. Phys. Chem. B* **2013**, *117*, 9380 – 9385.
[72] V. Tiwari, W. K. Peters, D. M. Jonas, *Proc. Natl. Acad. Sci. USA* **2013**, *110*, 1203 – 1208.
[73] C. C. Jumper, J. M. Anna, A. Stradomska, J. Schins, M. Myahkostupov, V. Prusakova, D. G. Oblinsky, F. N. Castellano, J. Knoester, G. D. Scholes, *Chem. Phys. Lett.* **2014**, *599*, 23 – 33.
[74] M. B. Plenio, J. Almeida, S. F. Huelga, *J. Chem. Phys.* **2013**, *139*, 235102.

[75] F. Milota, V. I. Prokhorenko, T. Mancal, H. von Berlepsch, O. Bixner, H. F. Kauffmann, J. Hauer, *J. Phys. Chem. A* **2013**, *117*, 6007 – 6014.
[76] D. Hayes, G. B. Griffin, G. S. Engel, *Science* **2013**, *340*, 1431 – 1434.
[77] A. Halpin, P. J. M. Johnson, R. Tempelaar, R. S. Murphy, J. Knoester, T. L. C. Jansen, R. J. D. Miller, *Nat. Chem.* **2014**, *6*, 196 – 201.
[78] V. Perlík, C. Lincoln, F. Šanda, J. Hauer, *J. Phys. Chem. Lett.* **2014**, *5*, 404 – 407.
[79] G. H. Richards, K. E. Wilk, P. M. G. Curmi, J. A. Davis, *J. Phys. Chem. Lett.* **2014**, *5*, 43 – 49.
[80] P. Nalbach, C. A. Mujica-Martinez, M. Thorwart, *Phys. Rev. E* **2015**, *91*, 022706.
[81] S. L. Logunov, V. V. Volkov, M. Braun, M. A. El-Sayed, *Proc. Natl. Acad. Sci. USA* **2001**, *98*, 8475 – 8479.
[82] D. S. Larsen, E. Papagiannakis, I. H. M. van Stokkum, M. Vengris, J. T. M. Kennis, R. van Grondelle, *Chem. Phys. Lett.* **2003**, *381*, 733 – 742.
[83] E. Papagiannakis, M. Vengris, D. S. Larsen, I. H. M. van Stokkum, R. G. Hiller, R. van Grondelle, *J. Phys. Chem. B* **2006**, *110*, 512 – 521.
[84] S. Draxler, T. Brust, S. Malkmus, J. A. DiGirolamo, W. J. Lees, W. Zinth, M. Braun, *Phys. Chem. Chem. Phys.* **2009**, *11*, 5019 – 5027.
[85] T. Wende, M. Liebel, C. Schnedermann, R. J. Pethick, P. Kukura, *J. Phys. Chem. A* **2014**, *118*, 9976 – 9984.
[86] D. J. Tannor, S. A. Rice, *J. Chem. Phys.* **1985**, *83*, 5013 – 5018.
[87] F. Gai, J. C. McDonald, P. A. Anfinrud, *J. Am. Chem. Soc.* **1997**, *119*, 6201 – 6202.
[88] S. Ruhman, B. Hou, N. Friedman, M. Ottolenghi, M. Sheves, *J. Am. Chem. Soc.* **2002**, *124*, 8854 – 8858.
[89] D. S. Larsen, I. H. van Stokkum, M. Vengris, M. A. van der Horst, F. L. de Weerd, K. J. Hellingwerf, R. van Grondelle, *Biophys. J.* **2004**, *87*, 1858 – 1872.
[90] G. Vogt, P. Nuernberger, T. Brixner, G. Gerber, *Chem. Phys. Lett.* **2006**, *433*, 211 – 215.
[91] P. Marquetand, P. Nuernberger, G. Vogt, T. Brixner, V. Engel, *Europhys. Lett. Publication of this title was ceased in 2006, please verify reference.***2007**, *80*, 53001.
[92] S. A. Rice, M. Zhao, *Optical Control of Molecular Dynamics*, Wiley-Interscience, New York, **2000**.
[93] P. W. Brumer, M. Shapiro, *Principles of the Quantum Control of Molecular Processes*, Wiley-Interscience, New York, **2003**.
[94] D. J. Tannor, *Introduction to Quantum Mechanics*: *A Time-Dependent Perspective*, University Science Books, Sausalito, **2007**.
[95] J. Bredenbeck, J. Helbing, P. Hamm, *J. Am. Chem. Soc.* **2004**, *126*, 990 – 991.
[96] J. Bredenbeck, J. Helbing, K. Nienhaus, G. U. Nienhaus, P. Hamm, *Proc. Natl. Acad. Sci. USA* **2007**, *104*, 14243 – 14248.
[97] J. Bredenbeck, J. Helbing, C. Kolano, P. Hamm, *ChemPhysChem* **2007**, *8*, 1747 – 1756.
[98] C. R. Baiz, M. J. Nee, R. McCanne, K. J. Kubarych, *Opt. Lett.* **2008**, *33*, 2533 – 2535.
[99] S. Ruetzel, M. Kullmann, J. Buback, P. Nuernberger, T. Brixner, *Phys. Rev. Lett.* **2013**, *110*, 148305.
[100] D. A. Blank, L. J. Kaufman, G. R. Fleming, *J. Chem. Phys.* **1999**, *111*, 3105 – 3114.
[101] S. Saito, I. Ohmine, *Phys. Rev. Lett.* **2002**, *88*, 207401.
[102] K. J. Kubarych, C. J. Milne, R. J. D. Miller, *Int. Rev. Phys. Chem.* **2003**, *22*, 497 – 532.
[103] W. Wohlleben, T. Buckup, J. L. Herek, M. Motzkus, *ChemPhysChem* **2005**, *6*, 850 – 857.
[104] P. Hamm, *J. Chem. Phys.* **2006**, *124*, 124506.
[105] F. Ding, M. T. Zanni, *Chem. Phys.* **2007**, *341*, 95 – 105.
[106] S. Garrett-Roe, P. Hamm, *Acc. Chem. Res.* **2009**, *42*, 1412 – 1422.
[107] A. F. Fidler, E. Harel, G. S. Engel, *J. Phys. Chem. Lett.* **2010**, *1*, 2876 – 2880.
[108] B. Brüggemann, T. Pullerits, *New J. Phys.* **2011**, *13*, 025024.
[109] Z. Zhang, K. L. Wells, H. Tan, *Opt. Lett.* **2012**, *37*, 5058 – 5060.
[110] M. Liebel, P. Kukura, *J. Phys. Chem. Lett.* **2013**, *4*, 1358 – 1364.
[111] T. Buckup, M. Motzkus, *Annu. Rev. Phys. Chem.* **2014**, *65*, 39 – 57.
[112] L. J. G. W. van Wilderen, A. T. Messmer, J. Bredenbeck, *Angew. Chem.* **2014**, *126*, 2705 – 2710.
[113] R. Kosloff, S. A. Rice, P. Gaspard, S. Tersigni, D. J. Tannor, *Chem. Phys.* **1989**, *139*, 201 – 220.
[114] P. Brumer, M. Shapiro, *Chem. Phys. Lett.* **1986**, *126*, 541 – 546.
[115] U. Gaubatz, P. Rudecki, M. Becker, S. Schiemann, M. Külz, K. Bergmann, *Chem. Phys. Lett.* **1988**, *149*, 463 – 468.
[116] R. S. Judson, H. Rabitz, *Phys. Rev. Lett.* **1992**, *68*, 1500 – 1503.
[117] C. J. Bardeen, V. V. Yakovlev, K. R. Wilson, S. D. Carpenter, P. M. Weber, W. S. Warren, *Chem. Phys. Lett.* **1997**, *280*, 151 – 158.
[118] K. Bergmann, H. Theuer, B. W. Shore, *Rev. Mod. Phys.* **1998**, *70*, 1003 – 1025.
[119] A. Assion, T. Baumert, M. Bergt, T. Brixner, B. Kiefer, V. Seyfried, M. Strehle, G. Gerber, *Science* **1998**, *282*, 919 – 922.
[120] D. Meshulach, Y. Silberberg, *Nature* **1998**, *396*, 239 – 242.
[121] J. L. Herek, W. Wohlleben, R. J. Cogdell, D. Zeidler, M. Motzkus, *Nature* **2002**, *417*, 533 – 535.
[122] T. Brixner, N. H. Damrauer, P. Niklaus, G. Gerber, *Nature* **2001**, *414*, 57 – 60.
[123] T. Brixner, G. Gerber, *ChemPhysChem* **2003**, *4*, 418 – 438.
[124] P. Nuernberger, G. Vogt, T. Brixner, G. Gerber, *Phys. Chem. Chem. Phys.* **2007**, *9*, 2470 – 2497.
[125] C. Brif, R. Chakrabarti, H. Rabitz, *New J. Phys.* **2010**, *12*, 075008.
[126] J. Hauer, T. Buckup, M. Motzkus, *Chem. Phys.* **2008**, *350*, 220 – 229.
[127] A. Weiner, D. Leaird, J. Patel, J. Wullert, *IEEE J. Quantum Electron.* **1992**, *28*, 908 – 920.
[128] A. M. Weiner, *Rev. Sci. Instrum.* **2000**, *71*, 1929 – 1960.
[129] A. M. Weiner, *Ultrafast Optics*, *1st ed.*, Wiley, Hoboken, **2009**.
[130] A. Monmayrant, S. Weber, B. Chatel, *J. Phys. B* **2010**, *43*, 103001.
[131] J. Arns, W. Colburn, S. Barden, *Curr. Dev. Opt. Des. Opt. Eng. VIII* **1999**, *3779*, 313 – 323.
[132] P. Blanche, P. Gailly, S. Habraken, P. Lemaire, C. Jamar, *Opt. Eng.* **2004**, *43*, 2603 – 2612.
[133] P. Nuernberger, R. Selle, F. Langhojer, F. Dimler, S. Fechner, G. Gerber, T. Brixner, *J. Opt. A* **2009**, *11*, 085202.
[134] I. Amat-Roldán, I. Cormack, P. Loza-Alvarez, E. Gualda, D. Artigas, *Opt. Express* **2004**, *12*, 1169 – 1178.
[135] A. Galler, T. Feurer, *Appl. Phys. B* **2008**, *90*, 427 – 430.
[136] A. Brodeur, S. L. Chin, *Phys. Rev. Lett.* **1998**, *80*, 4406.
[137] C. Nagura, A. Suda, H. Kawano, M. Obara, K. Midorikawa, *Appl. Opt.* **2002**, *41*, 3735 – 3742.
[138] M. Bradler, P. Baum, E. Riedle, *Appl. Phys. B* **2009**, *97*, 561 – 574.
[139] H. E. Lessing, A. V. Jena, *Chem. Phys. Lett.* **1976**, *42*, 213 – 217.
[140] U. Megerle, I. Pugliesi, C. Schriever, C. Sailer, E. Riedle, *Appl. Phys. B* **2009**, *96*, 215 – 231.
[141] S. Schott, A. Steinbacher, J. Buback, P. Nuernberger, T. Brixner, *J. Phys. B* **2014**, *47*, 124014.
[142] M. Rasmusson, A. N. Tarnovsky, E. Åkesson, V. Sundström, *Chem. Phys. Lett.* **2001**, *335*, 201 – 208.
[143] S. A. Kovalenko, A. L. Dobryakov, J. Ruthmann, N. P. Ernsting, *Phys. Rev. A* **1999**, *59*, 2369 – 2384.

[144] K. Ekvall, P. van der Meulen, C. Dhollande, L. Berg, S. Pommeret, R. Naskrecki, J. Mialocq, *J. Appl. Phys.* **2000**, *87*, 2340.
[145] M. Lorenc, M. Ziolek, R. Naskrecki, J. Karolczak, J. Kubicki, A. Maciejewski, *Appl. Phys. B* **2002**, *74*, 19 – 27.
[146] B. Dietzek, T. Pascher, V. Sundström, A. Yartsev, *Laser Phys. Lett.* **2007**, *4*, 38 – 43.
[147] S. M. Gallagher Faeder, D. M. Jonas, *J. Phys. Chem. A* **1999**, *103*, 10489 – 10505.
[148] L. P. DeFlores, R. A. Nicodemus, A. Tokmakoff, *Opt. Lett.* **2007**, *32*, 2966 – 2968.
[149] S. Shim, D. B. Strasfeld, Y. L. Ling, M. T. Zanni, *Proc. Natl. Acad. Sci. USA* **2007**, *104*, 14197 – 14202.
[150] K. F. Lee, A. Bonvalet, P. Nuernberger, M. Joffre, *Opt. Express* **2009**, *17*, 12379 – 12384.
[151] S. Shim, M. T. Zanni, *Phys. Chem. Chem. Phys.* **2009**, *11*, 748 – 761.
[152] J. A. Myers, K. L. Lewis, P. F. Tekavec, J. P. Ogilvie, *Opt. Express* **2008**, *16*, 17420 – 17428.
[153] P. F. Tekavec, J. A. Myers, K. L. M. Lewis, J. P. Ogilvie, *Opt. Lett.* **2009**, *34*, 1390 – 1392.
[154] H. Tan, *J. Chem. Phys.* **2008**, *129*, 124501.
[155] S. Yan, H. Tan, *Chem. Phys.* **2009**, *360*, 110 – 115.
[156] A. W. Albrecht, J. D. Hybl, S. M. G. Faeder, D. M. Jonas, *J. Chem. Phys.* **1999**, *111*, 10934 – 10956.
[157] J. Köhler, M. Wollenhaupt, T. Bayer, C. Sarpe, T. Baumert, *Opt. Express* **2011**, *19*, 11638 – 11653.
[158] P. F. Tekavec, J. A. Myers, K. L. M. Lewis, F. D. Fuller, J. P. Ogilvie, *Opt. Express* **2010**, *18*, 11015 – 11024.
[159] P. A. Tekavec, K. L. Lewis, F. D. Fuller, J. A. Myers, J. P. Ogilvie, *IEEE J. Sel. Top. Quantum Electron.* **2012**, *18*, 210 – 217.
[160] J. Buback, M. Kullmann, F. Langhojer, P. Nuernberger, R. Schmidt, F. Würthner, T. Brixner, *J. Am. Chem. Soc.* **2010**, *132*, 16510 – 16519.
[161] J. Buback, P. Nuernberger, M. Kullmann, F. Langhojer, R. Schmidt, F. Würthner, T. Brixner, *J. Phys. Chem. A* **2011**, *115*, 3924 – 3935.
[162] M. Kullmann, S. Ruetzel, J. Buback, P. Nuernberger, T. Brixner, *J. Am. Chem. Soc.* **2011**, *133*, 13074 – 13080.
[163] S. Ruetzel, M. Diekmann, P. Nuernberger, C. Walter, B. Engels, T. Brixner, *Proc. Natl. Acad. Sci. USA* **2014**, *111*, 4764 – 4769.
[164] S. Ruetzel, M. Diekmann, P. Nuernberger, C. Walter, B. Engels, T. Brixner, *J. Chem. Phys.* **2014**, *140*, 224310.
[165] C. Walter, S. Ruetzel, M. Diekmann, P. Nuernberger, T. Brixner, B. Engels, *J. Chem. Phys.* **2014**, *140*, 224311.
[166] C. Consani, S. Ruetzel, P. Nuernberger, T. Brixner, *J. Phys. Chem. A* **2014**, *118*, 11364 – 11372.
[167] J. C. Crano, R. J. Guglielmetti, *Organic Photochromic and Thermochromic Compounds*: *Physicochemical Studies*, *Biological Applications*, *and Thermochromism*, *Vol. 2*, *1st ed.*, Kluwer Academic, New York, **1999**.
[168] H. Dürr, H. Bouas-Laurent, *Photochromism*: *Molecules and Systems*, Elsevier, Amsterdam, **2003**.
[169] B. S. Lukyanov, M. B. Lukyanova, *Chem. Heterocycl. Compd.* **2005**, *41*, 281 – 311.
[170] D. Parthenopoulos, P. Rentzepis, *Science* **1989**, *245*, 843 – 845.
[171] G. Berkovic, V. Krongauz, V. Weiss, *Chem. Rev.* **2000**, *100*, 1741 – 1754.
[172] H. Bouas-Laurent, H. Dürr, *Pure Appl. Chem.* **2001**, *73*, 639 – 665.
[173] B. L. Feringa, *Molecular Switches*, Wiley-VCH, Berlin, **2001**.
[174] T. Stafforst, D. Hilvert, *Chem. Commun.* **2009**, 287 – 288.
[175] J. Kohl-Landgraf, M. Braun, C. Özcoban, D. P. N. Goṇcalves, A. Heckel, J. Wachtveitl, *J. Am. Chem. Soc.* **2012**, *134*, 14070 – 14077.
[176] M. Hammarson, J. R. Nilsson, S. Li, T. Beke-Somfai, J. Andréasson, *J. Phys. Chem. B* **2013**, *117*, 13561 – 13571.
[177] C. Özcoban, T. Halbritter, S. Steinwand, L. Herzig, J. Kohl-Landgraf, N. Askari, F. Groher, B. Fürtig, C. Richter, H. Schwalbe, B. Suess, J. Wachtveitl, A. Heckel, *Org. Lett.* **2015**, *17*, 1517 – 1520.
[178] Y. Futami, M. L. S. Chin, S. Kudoh, M. Takayanagi, M. Nakata, *Chem. Phys. Lett.* **2003**, *370*, 460 – 468.
[179] G. Cottone, R. Noto, G. L. Manna, S. L. Fornili, *Chem. Phys. Lett.* **2000**, *319*, 51 – 59.
[180] Y. Sheng, J. Leszczynski, A. A. Garcia, R. Rosario, D. Gust, J. Springer, *J. Phys. Chem. B* **2004**, *108*, 16233 – 16243.
[181] G. Cottone, R. Noto, G. L. Manna, *Molecules* **2008**, *13*, 1246 – 1252.
[182] M. Sanchez-Lozano, C. M. Estévez, J. Hermida-Ramón, L. Serrano-Andres, *J. Phys. Chem. A* **2011**, *115*, 9128 – 9138.
[183] R. Kobayashi, R. D. Amos, *Mol. Phys.* **2013**, *111*, 1574 – 1579.
[184] N. P. Ernsting, B. Dick, T. Arthen-Engeland, *Pure Appl. Chem.* **1990**, *62*, 1483 – 1488.
[185] N. Ernsting, T. Arthenengeland, *J. Phys. Chem.* **1991**, *95*, 5502 – 5509.
[186] A. K. Chibisov, H. Görner, *J. Phys. Chem. A* **1997**, *101*, 4305 – 4312.
[187] H. Görner, *Phys. Chem. Chem. Phys.* **2001**, *3*, 416 – 423.
[188] J. Hobley, U. Pfeifer-Fukumura, M. Bletz, T. Asahi, H. Masuhara, H. Fukumura, *J. Phys. Chem. A* **2002**, *106*, 2265 – 2270.
[189] A. Holm, M. Rini, E. T. J. Nibbering, H. Fidder, *Chem. Phys. Lett.* **2003**, *376*, 214 – 219.
[190] A. Holm, O. F. Mohammed, M. Rini, E. Mukhtar, E. T. J. Nibbering, H. Fidder, *J. Phys. Chem. A* **2005**, *109*, 8962 – 8968.
[191] C. J. Wohl, D. Kuciauskas, *J. Phys. Chem. B* **2005**, *109*, 22186 – 22191.
[192] E. Åkesson, H. Bergström, V. Sundström, T. Gillbro, *Chem. Phys. Lett.* **1986**, *126*, 385 – 393.
[193] Q. Xu, G. R. Fleming, *J. Phys. Chem. A* **2001**, *105*, 10187 – 10195.
[194] P. Nuernberger, G. Vogt, G. Gerber, R. Improta, F. Santoro, *J. Chem. Phys.* **2006**, *125*, 044512.
[195] G. Vogt, P. Nuernberger, G. Gerber, R. Improta, F. Santoro, *J. Chem. Phys.* **2006**, *125*, 044513.
[196] B. Dietzek, T. Pascher, A. Yartsev, *J. Phys. Chem. B* **2007**, *111*, 6034 – 6041.
[197] B. Dietzek, A. Yartsev, A. N. Tarnovsky, *J. Phys. Chem. B* **2007**, *111*, 4520 – 4526.
[198] A. Weigel, M. Pfaffe, M. Sajadi, R. Mahrwald, R. Improta, V. Barone, D. Polli, G. Cerullo, N. P. Ernsting, F. Santoro, *Phys. Chem. Chem. Phys.* **2012**, *14*, 13350 – 13364.
[199] I. H. M. van Stokkum, D. S. Larsen, R. van Grondelle, *Biochim. Biophys. Acta Bioenerg.* **2004**, *1657*, 82 – 104.
[200] R. Williams, *Appl. Spectr. Rev.* **1989**, *25*, 63 – 79.
[201] V. Cervetto, J. Helbing, J. Bredenbeck, P. Hamm, *J. Chem. Phys.* **2004**, *121*, 5935 – 5942.
[202] A. Nemeth, F. Milota, J. Sperling, D. Abramavicius, S. Mukamel, H. F. Kauffmann, *Chem. Phys. Lett.* **2009**, *469*, 130 – 134.
[203] F. Milota, J. Sperling, A. Nemeth, H. Kauffmann, *Chem. Phys.* **2009**, *357*, 45 – 53.
[204] M. Cho, H. M. Vaswani, T. Brixner, J. Stenger, G. R. Fleming, *J. Phys. Chem. B* **2005**, *109*, 10542 – 10556.
[205] A. V. Pisliakov, T. Mancal, G. R. Fleming, *J. Chem. Phys.* **2006**, *124*, 234505.
[206] P. Kjellberg, B. Brüggemann, T. Pullerits, *Phys. Rev. B* **2006**, *74*, 024303.
[207] F. Milota, J. Sperling, A. Nemeth, T. Mancal, H. F. Kauffmann, *Acc. Chem. Res.* **2009**, *42*, 1364 – 1374.

[208] S. Yang, H. Tian, H. Xiao, X. Shang, X. Gong, S. Yao, K. Chen, *Dyes Pigm.* **2001**, *49*, 93 – 101.
[209] C. J. Bardeen, Q. Wang, C. V. Shank, *Phys. Rev. Lett.* **1995**, *75*, 3410 – 3413.
[210] G. Cerullo, C. J. Bardeen, Q. Wang, C. V. Shank, *Chem. Phys. Lett.* **1996**, *262*, 362 – 368.
[211] C. J. Bardeen, J. Che, K. R. Wilson, V. V. Yakovlev, V. A. Apkarian, C. C. Martens, R. Zadoyan, B. Kohler, M. Messina, *J. Chem. Phys.* **1997**, *106*, 8486 – 8503.
[212] C. J. Bardeen, Q. Wang, C. V. Shank, *J. Phys. Chem. A* **1998**, *102*, 2759 – 2766.
[213] C. Bardeen, V. Yakovlev, J. Squier, K. Wilson, *J. Am. Chem. Soc.* **1998**, *120*, 13023 – 13027.
[214] K. Misawa, T. Kobayashi, *J. Chem. Phys.* **2000**, *113*, 7546.
[215] T. Chen, A. Vierheilig, P. Waltner, M. Heid, W. Kiefer, A. Materny, *Chem. Phys. Lett.* **2000**, *326*, 375 – 382.
[216] T. Hellerer, A. M. K. Enejder, A. Zumbusch, *Appl. Phys. Lett.* **2004**, *85*, 25 – 27.
[217] K. P. Knutsen, J. C. Johnson, A. E. Miller, P. B. Petersen, R. J. Saykally, *Chem. Phys. Lett.* **2004**, *387*, 436 – 441.
[218] S. Malkmus, R. Dürr, C. Sobotta, H. Pulvermacher, W. Zinth, M. Braun, *J. Phys. Chem. A* **2005**, *109*, 10488 – 10492.
[219] G. Vogt, P. Nuernberger, R. Selle, F. Dimler, T. Brixner, G. Gerber, *Phys. Rev. A* **2006**, *74*, 033413.
[220] M. P. A. Branderhorst, P. Londero, P. Wasylczyk, C. Brif, R. L. Kosut, H. Rabitz, I. A. Walmsley, *Science* **2008**, *320*, 638 – 643.
[221] S. Ruhman, R. Kosloff, *J. Opt. Soc. Am. B* **1990**, *7*, 1748 – 1751.
[222] D. Wolpert, M. Schade, F. Langhojer, G. Gerber, T. Brixner, *J. Phys. B* **2008**, *41*, 074025.
[223] P. Nuernberger, *Opt. Commun.* **2009**, *282*, 227 – 235.
[224] S. Ruetzel, C. Stolzenberger, S. Fechner, F. Dimler, T. Brixner, D. J. Tannor, *J. Chem. Phys.* **2010**, *133*, 164510.
[225] A. Konar, V. V. Lozovoy, M. Dantus, *J. Phys. Chem. Lett.* **2012**, *3*, 2458 – 2464.
[226] A. Konar, V. V. Lozovoy, M. Dantus, *J. Phys. Chem. Lett.* **2014**, *5*, 924 – 928.
[227] T. Zhang, C. Borca, X. Li, S. Cundiff, *Opt. Express* **2005**, *13*, 7432 – 7441.
[228] A. D. Bristow, D. Karaiskaj, X. Dai, T. Zhang, C. Carlsson, K. R. Hagen, R. Jimenez, S. T. Cundiff, *Rev. Sci. Instrum.* **2009**, *80*, 073108.
[229] R. Augulis, D. Zigmantas, *Opt. Express* **2011**, *19*, 13126 – 13133.
[230] F. Milota, C. N. Lincoln, J. Hauer, *Opt. Express* **2013**, *21*, 15904.
[231] Y. Zhang, K. Meyer, C. Ott, T. Pfeifer, *Opt. Lett.* **2013**, *38*, 356.
[232] I. A. Heisler, R. Moca, F. V. A. Camargo, S. R. Meech, *Rev. Sci. Instrum.* **2014**, *85*, 063103.
[233] H. Zheng, J. R. Caram, P. D. Dahlberg, B. S. Rolczynski, S. Viswanathan, D. S. Dolzhnikov, A. Khadivi, D. V. Talapin, G. S. Engel, *Appl. Opt.* **2014**, *53*, 1909.
[234] B. Spokoyny, E. Harel, *J. Phys. Chem. Lett.* **2014**, *5*, 2808 – 2814.
[235] B. Spokoyny, C. J. Koh, E. Harel, *Opt. Lett.* **2015**, *40*, 1014 – 1017.
[236] A. A. Haddad, A. Chauvet, J. Ojeda, C. Arrell, F. van Mourik, G. Auböck, M. Chergui, *Opt. Lett.* **2015**, *40*, 312.
[237] R. D. Mehlenbacher, T. J. McDonough, M. Grechko, M. Wu, M. S. Arnold, M. T. Zanni, *Nat. Commun.* **2015**, *6*, 6732.
[238] B. A. West, P. G. Giokas, B. P. Molesky, A. D. Ross, A. M. Moran, *Opt. Express* **2013**, *21*, 2118 – 2125.
[239] G. Auböck, C. Consani, R. Monni, A. Cannizzo, F. van Mourik, M. Chergui, *Rev. Sci. Instrum.* **2012**, *83*, 093105.
[240] F. Kanal, S. Keiber, R. Eck, T. Brixner, *Opt. Express* **2014**, *22*, 16965 – 16975.
[241] E. Harel, A. F. Fidler, G. S. Engel, *Proc. Natl. Acad. Sci. USA* **2010**, *107*, 16444 – 16447.
[242] E. Harel, A. F. Fidler, G. S. Engel, *J. Phys. Chem. A* **2011**, *115*, 3787 – 3796.

Received: March 31, 2015
Published online: August 26, 2015